# Fragmentation reactions of thiourea- and urea-compounds examined by tandem MS-, energy-resolved CID experiments, and theory

Francesco Falvo,[a] Lukas Fiebig,[a] Frank Dreiocker,[a] Ran Wang,[b] P. B. Armentrout,[b] and Mathias Schäfer[a,*]

[a]*Department of Chemistry, Institute of Organic Chemistry, University of Cologne, Greinstraße 4, 50939 Köln, Germany*
*Tel. ++49(0)2214703086; Fax: ++49 (0)2214703064*
[b]*Department of Chemistry, University of Utah, Salt Lake City, Utah, USA.*
*Correspondence to **Mathias Schäfer**: mathias.schaefer@uni-koeln.de

**Keywords**
Collision induced dissociation, energy-dependent dissociation, breakdown curve, reaction mechanism, computational modeling

**Abstract**

Fragmentation reactions of thiourea- and urea-compounds, which are promising reagents for chemical crosslinking (XL), are investigated in detail by collision-induced dissociation (CID) experiments in a quadrupole ion trap (QIT), energy-resolved CID experiments, and computational modeling. For this study, an array of six labeled and unsymmetrical substituted thiourea- and urea-derivatives were synthesized, which allow unambiguous characterization of competing fragmentation pathways. The results of the QIT-CID-experiments are explored in detail for two compounds and confirmed by results for the other four. These results document the subtle competition of characteristic fragmentation pathways of this class of compounds. The multi dimensional investigations of the characteristic fragmentation reactions allow reliable structure proposals of prominent product ions. Energy-dependent CID experiments on two of the six compounds lead to breakdown curves that show similar relative threshold energies for the formation of the product ions on which the functioning of the XL application relies. The experimental results are in full consistency with the results from in-depth computations. For the dominant fragmentations observed, the transition states for moving the proton from the most basic site of the precursor ion (the thiourea-sulphur or the urea carbonyl oxygen) to less basic heteroatoms in the protonated molecular ion is the necessary and decisive step that determines the extent of the charge-driven fragmentation processes that follow.

## 1. Introduction

Chemical cross linking (XL) is an established analytical strategy to study three-dimensional protein structures and to map protein interfaces [1-4]. However, the unambiguous, sensitive, and rapid identification of chemically modified amino acids in complex peptide mixtures after enzymatic digestion is challenging as only a relatively low amount of cross-linked products are present along with a large majority of unmodified peptides. Tailor-made cross linkers that fragment readily upon collisional activation offer a solution for this problem as they give rise to characteristic fragment ions or show characteristic neutral losses that in turn afford facile and reliable tandem mass spectrometric analysis [5-11]. Recently, we have introduced urea- and thiourea-compounds


UU IR Author Manuscript

for XL that are especially suited for collision-induced dissociation (CID) analysis (see compounds **7a** and **7b** in Scheme 1) [5-7, 11]. Their typical and highly preferred fragmentation reactions, which make them effective CID-labile XL-reagents, are the fragmentation of the urea-moiety and the cleavage of an amide bond adjacent to the thiourea-moiety [6, 11]. These different competing fragmentation reactions, their mechanisms, and the structure of their key product ions are examined here in detail [12, 13].

The rather new application as efficient XL-reagents was adapted from the well documented nucleophilic reactivity of the thiourea sulphur of *N*-terminal phenyl thiocarbamoyl compounds, which is essential for the *Edman* degradation reaction [5, 14] and also the basis for ladder sequencing of peptides by MS/MS [15, 16]. In addition, urea- and thiourea-compounds have attracted attention as potent organocatalysts because of their effective influence on reactions via their unique hydrogen-bonding patterns [17-22]. Finally, the urea-moiety is frequently found in pseudopeptides, which are interesting new biodegradable polymeric materials for biomedical applications [23]. Most importantly, urea is the main nitrogen-containing substance in the urine of mammals as it is the major end product of nitrogen metabolism and as such a ubiquitous compound of biochemical importance [24].

In this contribution, we turn our attention to the fundamentals of the characteristic CID pathways of protonated and sodiated alkyl thiocarbamoyl and alkyl carbamoyl molecular ions to ultimately understand and evaluate the obvious differences in reactivity of urea and thiourea vs. simple amide moieties in the gas phase. To accomplish this complex analytical task, we first synthesized a set of unsymmetrical thiourea- and urea-compounds, **1** - **6** shown in Scheme 1, which are simplified analogues of the reagents used for XL, **7a** and **7b**. These compounds allow unambiguous identification of the competing fragmentation reactions on the basis of characteristic product ions generated in quadrupole ion traps (QIT) $MS^n$ product ion experiments. As illustrated in Scheme 1, compounds **1** and **2** are deuterium labeled thiocarbamoyl- and carbamoyl-derivatives that come with the key structural features also present in the XL-reagents, i.e., an alkyl thiourea/urea moiety connected to butyric acid amides (see compounds **7a** and **7b** in Scheme 1) [6, 11]. As this pair of derivatives shows only a minimal structural difference, the discussion of the analytical results is focused on them, but results for compounds **3**-**6** are considered as well. The structures of compounds **3**-**6** differ more substantially as they are decorated with diverse alkyl groups (propyl and cyclohexyl) and even with a glycylmethylester-moiety (compound **4**). These compounds are included in the study to probe if subtle differences in inductive and steric effects, which can be expected from the presence of differing alkyl groups (R and R'), have an influence on the fragmentation pathways. These results allow further evaluation of the experimental findings for compounds **1** and **2**.

The fragmentation behavior of protonated and sodiated molecular ions of the model compounds **1**-**6** was examined by electrospray ionization (ESI)-MS/MS in a QIT. The energetics of the dissociation reactions of compounds **1** and **2** are subsequently probed by energy-resolved QIT-CID experiments and by computational modeling [25-30]. The energy-dependent CID experiments yield breakdown curves that allow the approximate determination of relative appearance energies of product ions, which are then compared to predictions by theory [25, 26, 29, 30].

UU IR Author Manuscript

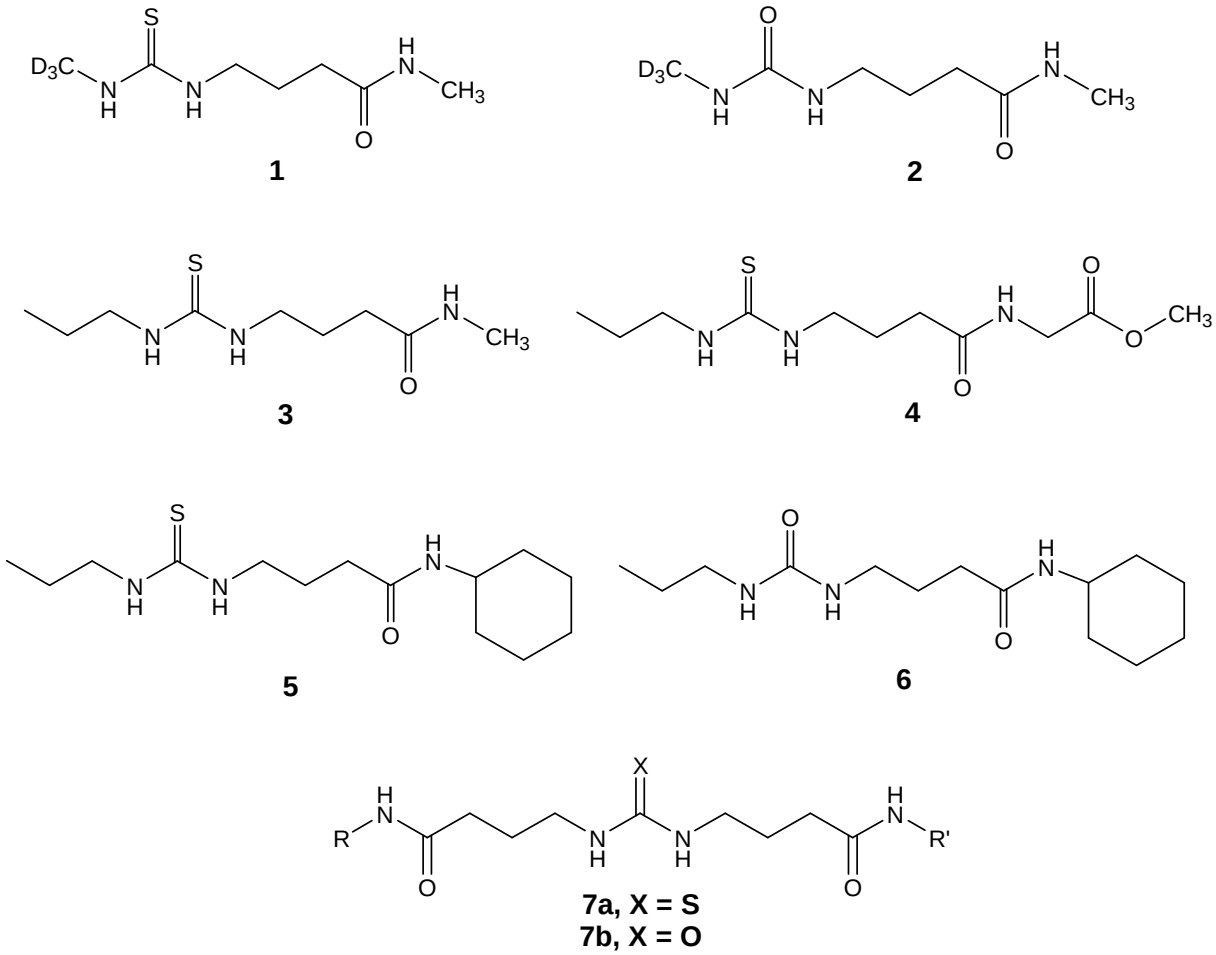


**Scheme 1:** Alkyl thiourea and alkyl urea compounds **1**-**6** examined in this work. Symmetric CID-labile XL-reagents **7a** (X = S) and **7b** (X = O) are presented here for structural comparison. XL-reagents **7a** and **7b**, are initially activated amine sensitive *N*-hydroxy succinimide (NHS) ester, which are shown here after condensation reaction with peptide amine moieties (R and R').

## 2. Materials and Methods

### 2.1. Mass Spectrometry

All chemicals and solvents were used as purchased without further purification (*Acros Organics, Aldrich, Fluka, Merck* and *Lancaster*). Tandem-MS CID-experiments with monoisotopic precursor ion selection (conducted with the magnetic (B) and electric (E) sectors, i.e., the BE part) were carried out in the quadrupole ion trap (QIT) of a hybrid BE-QIT *Finnigan* MAT 900 mass spectrometer (*ThermoFisher Scientific*, Bremen). Exact ion masses of all protonated and sodiated precursor ions as well as of the $MS^n$ product ions were measured in the orbitrap analyzer of a LTQ Orbitrap XL instrument at resolutions > 30000 FWHH (*ThermoFisher Scientific*, Bremen). The theoretical masses of all ions discussed match the exact ion masses determined (external calibration: $\Delta m \leq 3$ppm; internal standards: $\leq$ 1ppm).

Energy-resolved $MS^2$ experiments were conducted on a Bruker Esquire 3000 plus ion trap mass spectrometer (*Bruker Daltonics GmbH*, Bremen, Germany) equipped with an electrospray ionization (ESI) source yielding the breakdown curves shown below. 50 $MS^2$

product ion spectra were acquired at every activation voltage and the ion abundances were averaged to yield the respective data points presented below. Nitrogen was used as the drying and nebulizer gas at a temperature of 295 °C, a flow rate of 5 l/min, and a back-pressure of 10 psi. The needle voltage was always set to 4 kV. Protonated precursor ions of compounds **1** and **2** were generated in the gas phase by introducing a $10^{-6}$ M methanolic solution of the analyte with 0.1 vol% trifluoroacetic acid into the ESI source at a flow rate of 9 µl/min. Breakdown curves were determined by monoisotopic mass selection of the corresponding parent ion and applying an activation voltage for a period of 20 ms. Helium was used as the collision gas. Activation voltages then were increased in a stepwise fashion until complete dissociation of the ion of interest was observed.

**2.2. Synthesis of *N*-Methyl-4-(3-trideuteromethyl-thioureido)-butyramide (1)**

*Tert*-butyloxycarbonyl (BOC) protection of the amine functionality of 4-aminobutyric acid (5 g; 48.5 mmol) was achieved by reaction with di-*tert*-butyl dicarbonate (22.21 g; 101.8 mmol) and triethylamine (29.45 g; 291 mmol) in methanol in 10 h [31]. After the evaporation of the solvent, the residual oil was dissolved in 150 ml saturated sodium hydrogen carbonate solution and extracted with ethylacetate. The aqueous phase was acidified with 1 N HCl to pH 2-3 and also extracted with ethylacetate. The combined organic layers were dried over magnesium sulfate and finally a white solid was obtained.

A mixture of the BOC-protected amino acid (2.3 g; 10 mmol), methylamine hydrochloride (0.81 g; 12 mmol), and triethylamine (3.54 g; 35 mmol) in 200 ml dichloromethane was cooled to 0 °C. Then a 1-propanephosphonic acid cyclic anhydride (T3P) solution in dimethyl formamide (DMF, 50 % w/w) was added drop wise and the mixture was allowed to warm to room temperature overnight [32]. The mixture was washed with 1 N HCl, 1 N NaOH, saturated sodium chloride solution and dried over magnesium sulfate. After evaporation of the solvent, *tert*-butyl 4-(methylamino)-4-oxobutylcarbamate was isolated as a colorless solid.

The BOC-deprotection (1.2 g; 5.6 mmol) was carried out in trifluoroacetic acid within one hour at room temperature. The solution was evaporated to dryness in vacuo and the residue triturated with dry diethyl ether. The residual oil was disintegrated under fresh diethylether, filtered and dried in vacuo. The resulting colorless oil was used without purification.

For the synthesis of the isothiocyanate, 1.19 g of the amine (5 mmol) were dissolved in a mixture of acetonitrile and carbon disulfide (0.4 g; 5.25 mmol). After slowly adding 1.21 g of triethylamine (11.5 mmol), the reaction mixture was stirred for 20 min before methyl chloroformate (0.57 g; 5.6 mmol) was added. After refluxing for 3 h, the mixture was cooled down to room temperature and poured into water [33]. The organic layer was washed with diluted hydrochloric acid and brine, dried over magnesium sulfate and concentrated under reduced pressure. The resulting yellowish oil was purified by column chromatography with ethyl acetate/cyclohexane (2:1) and 0.61 g of the product was isolated as colorless oil (73%).

For the reaction of the isothiocyanate with trideutero methylamine hydrochloride (0.07 g; 1 mmol), the amine was suspended in 15ml acetonitrile and treated with 0.11 g triethylamine (1.05 mmol). After 15 min, 0.16 g of the isothiocyanate (1 mmol) were added at 0 °C and the reaction mixture was brought to 20 °C within 20 h. After the evaporation of the solvent, the crude product was purified by column chromatography with dichloromethane/methanol (10:1). The methyl thiocarbamoyl-derivative **1** was isolated as a colorless solid (0.17 g; 88%).

**2.3. Synthesis of *N*-Methyl-4-(3-trideuteromethyl-ureido)-butyramide (2)**

Compound **1** was dissolved in an aqueous sodium hydroxide solution. After 10 min a 35 % hydrogen peroxide solution was added drop wise at 0 °C to the reaction mixture and the mixture was allowed to warm to room temperature over night [34]. After evaporation to dryness the raw product was purified by column chromatography with dichloromethane/methanol (5:1). Compound **2** was isolated as a colorless solid (0.05 g; 68%).

**2.4. Synthesis of *N*-Methyl-4-(3-propyl-thioureido)-butyramide (3)**

The synthesis of compound **3** was carried out by the reaction of the corresponding isothiocyanate (see synthesis of compound **1**) with propylamine.

**2.5. Synthesis of [4-(3-Propyl-thioureido)-butyrylamino]-acetic acid methyl ester (4)**

A mixture of 5 g BOC-protected 4-aminobutyric acid (25mmol), 3.61 g 4-dimethylaminopyridine (DMAP; 30 mmol), 4.3 g glycine methylester hydrochloride (34 mmol), and 4.34 g triethylamine (43 mmol) in dichloromethane was cooled to 0 °C. 7.11 g Dicyclohexyl carbodiimide (DCC; 34 mmol) were added after 20 min and the mixture was warmed up to room temperature over night. The mixture was washed with 1 N HCl, 1 N NaOH, saturated sodium chloride solution and dried over magnesium sulfate. After evaporation of the solvent, 5.6 g (82%) of the crude product were purified by column chromatography with dichloromethane/methanol (10:1) as a white solid.

Cleavage of the BOC-group occurs in trifluoroacetic acid within one hour at room temperature. The resulting amine-salt was converted to the respective isothiocyanate as described above. The reaction of 0.916 g isothiocyanate (4.24 mmol) with 0.5 g propylamine (8.47 mmol) leads to thiourea-derivative **4** (0.962 g; 83%).

**2.6. Synthesis of *N*-Cyclohexyl-4-(3-propyl-thioureido)-butyramide (5)**

Compound **5** (0.015 g; 59%) was synthesized in analogy to compound **3**.

**2.7. Synthesis of *N*-Cyclohexyl-4-(3-propyl-ureido)-butyramide (6)**

Compound **6** (0.066 g; 98%) was synthesized in analogy to compound **2**.

**2.8. Computations**

To find the global energy minimum and all low-energy geometries, a large number of possible conformations were screened using a simulated annealing methodology with the AMBER program and the AMBER force field based on molecular mechanics [35]. All possible structures identified this way were subsequently optimized using NWChem [36] at the HF/3-21G level [37, 38]. Unique structures for each system were optimized using Gaussian 09 [39] at the B3LYP/6-31G(d,p) level of theory [40, 41] with the “loose” keyword (maximum step size 0.01 au and an RMS force of 0.0017 au) to facilitate convergence. A series of relaxed potential energy surface (PES) scans at the B3LYP/6-31+G(d) level were performed to locate transition state and intermediate structures occurring along the potential energy surfaces for fragmentation. Unique structures of all stable conformations, intermediates, transition states, and products obtained from these procedures were then chosen for higher-level geometry optimization and frequency calculations using the B3LYP/6-311+G(d,p) level of

theory [42]. Each transition state was found to contain one imaginary frequency and each intermediate was vibrationally stable. Vibrational frequencies were also calculated at this level and were scaled by 0.99 [43] in determining zero-point vibrational energy (ZPE) corrections. Single-point energies were determined at the B3LYP, B3P86, and MP2(full) levels using the 6-311+G(2d,2p) basis set and the B3LYP/6-311+G(d,p) geometries.

## 3. Results and Discussion

### 3.1. (+)ESI-QIT-$MS^2$-experiments

#### 3.1.1. Protonated molecular ion of compound 1: $[1 + H]^+$

The major fragmentation pathway of the protonated molecular ion of compound **1** at *m/z* 193 is the cleavage of the thiourea moiety, i.e., loss of trideutero methylamine $CD_3NH_2$ (Δm 34u) to generate the product ion at *m/z* 159 (see Figure 1). Additionally, the loss of methylamine $CH_3NH_2$ (Δm 31u) leading to formation of a product ion at *m/z* 162 is found in the $MS^2$-spectrum of model compound **1** with moderate abundance (Figure 1). In both cases, plausible mechanisms include backside nucleophilic attack either of the carbonyl oxygen onto the thiocarbonyl or of the thiourea carbonyl sulphur onto the amide carbonyl group, respectively, leading to 7-membered heterocyclic products (Scheme 2). Alternatively, simple loss of $CD_3NH_2$ would form a product ion stabilized by a hydrogen bond between the thioisocyanate nitrogen and the amide oxygen (*m/z* 159), as Scheme 2 illustrates. Loss of $CH_3NH_2$ can lead to at least three different product ion structures found at *m/z* 162: (a) the 7-membered heterocyclic product ion, (b) a protonated γ-butyrolactame-derivative formed by nucleophilic attack of the thiourea nitrogen onto the amide carbonyl carbon, and finally (c) a rather unstable acylium ion, Scheme 2. These suggestions are derived from the broadly accepted understanding of peptide backbone amide bond fragmentation reaction mechanisms, which were elucidated by MS/MS experiments and in-depth computations [44-47]. In particular protonated oxazolone *b*-ions formed by nucleophilic attack of adjacent carbonyl oxygens and cleavage of an amide bond are reliably confirmed and explain the observed stability of peptide *b*-ions [48]. However, acylium *b*-ions, which were hypothesized at early stages of the research, have been subsequently clearly disproved as such ions are very unstable because of the facile exothermic loss of carbon monoxide, which converts them into much more stable immonium *a*-ions [49]. Even though the product ion at *m/z* 162 is not derived from a protonated α-amino acid and therefore a stable immonium *a*-ion analogue cannot be formed by CO loss (a product not found in the $MS^2$ spectrum), we favour a 7-membered ring over an acylium ion structure for *m/z* 162 (see Scheme 2). Although nucleophilic attack of the thiourea sulphur cleaving off the neighbouring amide bond is the characteristic and predominant reaction of the thiourea-XL reagent (compound **7a** in Scheme 1), this fragmentation pathway is outmatched by the cleavage of the thiourea-moiety in protonated molecular ions of compound **1** (see Figure 1, Scheme 2) [6].

A third charge-driven fragmentation reaction, i.e., the loss of trideutero methyl isothiocyanate $CD_3NCS$ (Δm 76u) is found in the $MS^2$-spectrum of $[\mathbf{1} + H]^+$ (see Scheme 2 and Figure 1), the analogue of which (loss of 101u) is also found for $[\mathbf{5} + H]^+$ (see SI: Scheme 1S and Figure 6S). The former reaction leads to the protonated 4-amino-*N*-methyl-butyramide ion at *m/z* 117, which can further fragment to yield ions at *m/z* 110 and 86 upon loss of ammonia and methylamine, respectively (see also SI: Figure 1S). The *m/z* 100 product could also be formed directly from $[\mathbf{1} + H]^+$ by loss of $CD_3NHCSNH_2$ (methyl thiourea, Δm 93u)

induced by nucleophilic attack of the oxygen at the urea nitrogen, Scheme 2. Computations suggest that the most likely pathway for formation of *m/z* 86 is by loss of $CD_3NCS$ from the γ-butyrolactame structure of *m/z* 162.

To understand the occurrence of QIT secondary fragmentation processes, it is appropriate to recall the basics of ion activation and fragmentation in QIT-MS in which only a selected precursor ion is in resonance with the radiofrequency applied for activation. This interaction increases the kinetic energy of the precursor ion and the multiple collisions with the He-buffer gas lead to accumulation of internal energy via the slow heating mechanism of activation and eventually to CID [50]. All product ions generated by primary fragmentation of the precursor ion are then rapidly cooled by dissipative low energy collisions with the He background gas [51-53]. This is certainly true for low collision energies, whereas high collision energies lead to "hot" fragment ions that can dissociate further before being effectively cooled by the helium in the trap [54, 55]. In Figure 1 as well as in the other QIT-$MS^2$ product ion spectra shown in this contribution, the precursor ions are completely depleted and therefore increased collision energies were applied. Hence, in addition to primary fragmentation of the activated precursor ion, secondary fragmentation reactions of product ions can also occur, as frequently found at sufficiently high activation energies deposited into resonantly excited precursor ions.

All charge-driven fragmentation reactions shown in Scheme 2 rely on the ionizing proton to be located adjacent to the covalent bond that is to be cleaved. The distribution of the proton over various sites of different basicity in the molecular ion that is the precondition for all of the subsequent cleavages can be understood by the mobile proton model [44, 46, 47, 56-63]. According to this concept, the proton migrates upon collisional activation (CA) from the most basic site in the precursor ion, in this case the thiourea-sulphur, to the decisive location for each of the discussed charge-driven fragmentation reactions, as indicated in Scheme 2. (In this context and throughout the remainder of the paper, we use the term CA to indicate activated steps that occur before dissociation.)

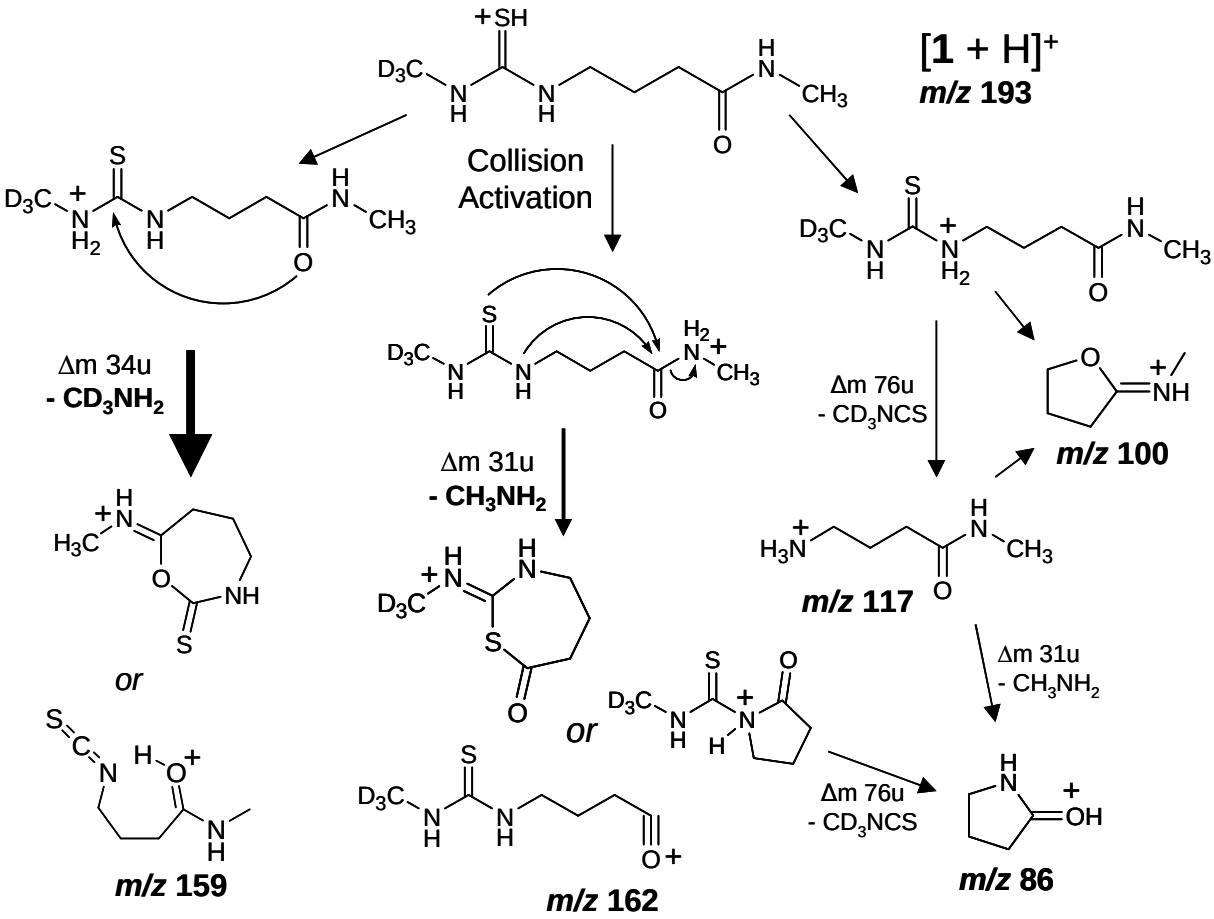


**Scheme 2:** Charge-driven fragmentation pathways observed in the (+)ESI-QIT-MS$^2$ product ion spectrum of the protonated molecular ion [**1** + H]$^+$ of **1** at *m/z* 193 (see Figure 1).

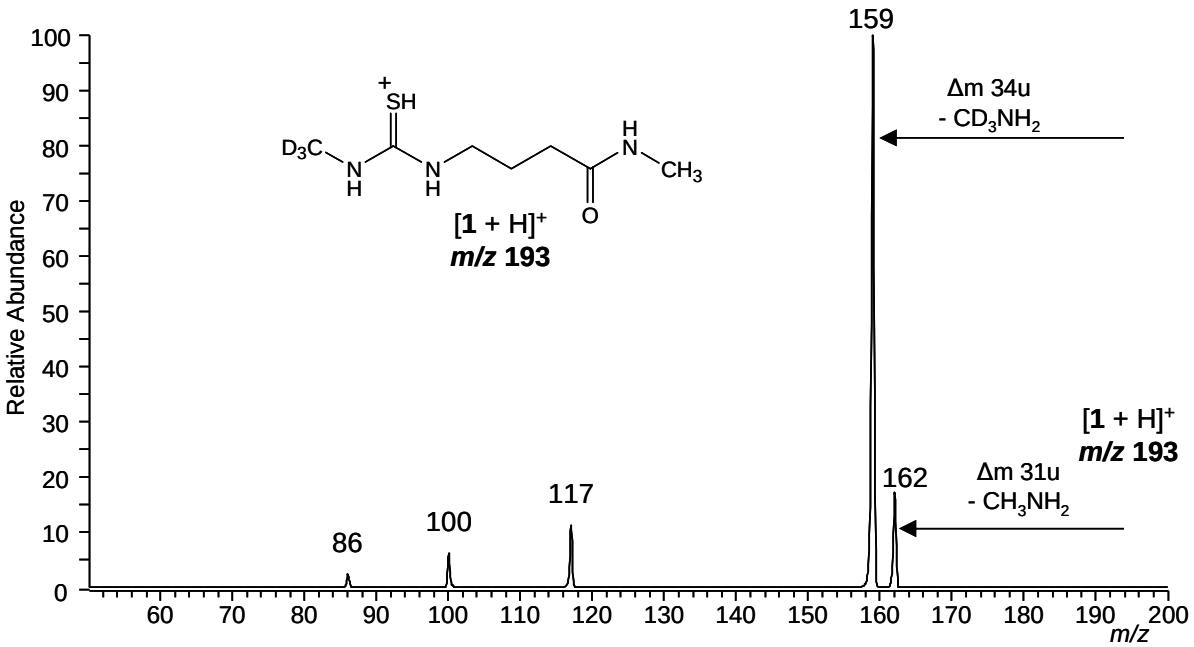


**Figure 1:** (+)ESI-QIT-MS$^2$ product ion spectrum of the protonated precursor ion [**1** + H]$^+$ at *m/z* 193. The precursor ion is completely depleted by CID.

### 3.1.2. Sodiated molecular ion of compound 1: $[1 + Na]^+$

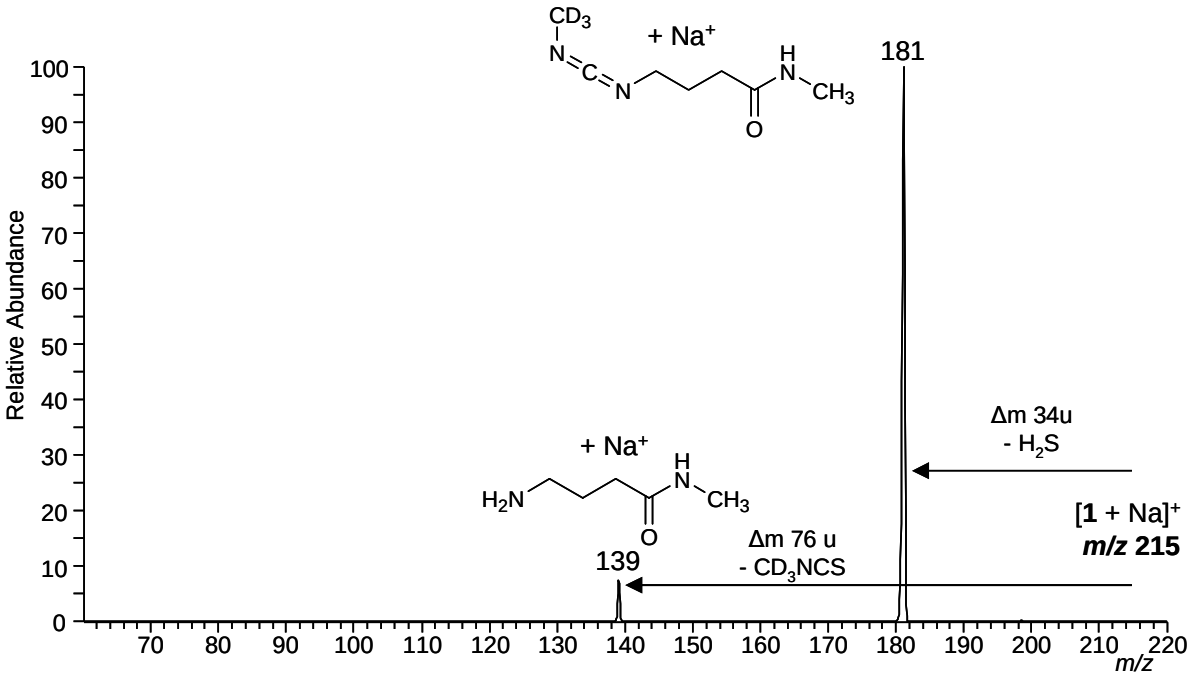


**Figure 2:** ESI-QIT-$MS^2$-product ion spectrum of the sodiated precursor ion [**1** + Na]$^+$ at *m/z* 215. The precursor ion is completely depleted by CID.

In analogy with protonated **1**, sodiated **1** also loses 34 u predominantly and 76 u in lower abundance upon collisional activation. However, exact ion mass determination of the sodiated precursor ion [**1** + Na]$^+$ at *m/z* 215 and the product ion (*m/z* 181) proves that the respective mass shift of 34 u originates from the loss of hydrogen sulfide and not of $CD_3NH_2$ (compare Figure 1 & Scheme 2). To rationalize the loss of $H_2S$ and the formation of the sodiated carbodiimide ion at *m/z* 181 starting from the sodiated thiourea-compound **1**, we assume a preceding tautomerization upon CA that converts the predominant *thione* to the respective *enthiol* tautomer, which then eventually cleaves off $H_2S$ in a subsequent fragmentation reaction (Scheme 3) [64]. The elimination of hydrogen sulfide from the sodiated precursor ion evidences the importance of the ionizing proton for the loss of $CD_3NH_2$, which is absent in this case (SI: Scheme 2S). However, the loss of trideutero methyl isothiocyanate $CD_3NCS$ depends on a hydrogen shift to form the sodiated 4-amino-*N*-methyl-butyramide at *m/z* 139. The loss of $H_2S$ is found in all QIT-$MS^2$ product ion spectra of sodiated thiourea-compound precursor ions (i.e., compounds **3**-**5**; see SI: Figures 2S, 5S, 7S and Scheme 2S), which was additionally confirmed by H/D exchange experiments with compound **5** (loss of Δm 36u = $D_2S$ for CID of the triply deuterated [$D_3$**5** + Na]$^+$ molecular ion; SI: Figure 10S).

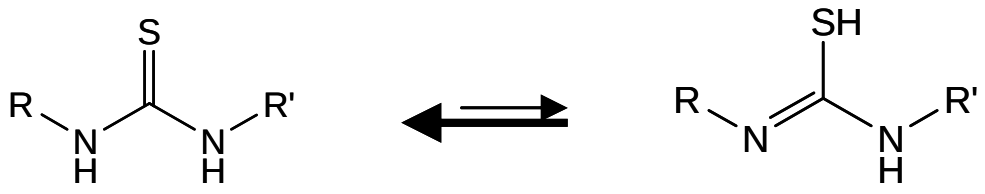

**Scheme 3:** *Thione-enthiol* tautomerization of thiourea-compounds. In solution and in the gas phase, the equilibrium lies predominantly on the left side at the thione [64].

### 3.1.3. Protonated molecular ion of compound 2: $[2 + H]^+$

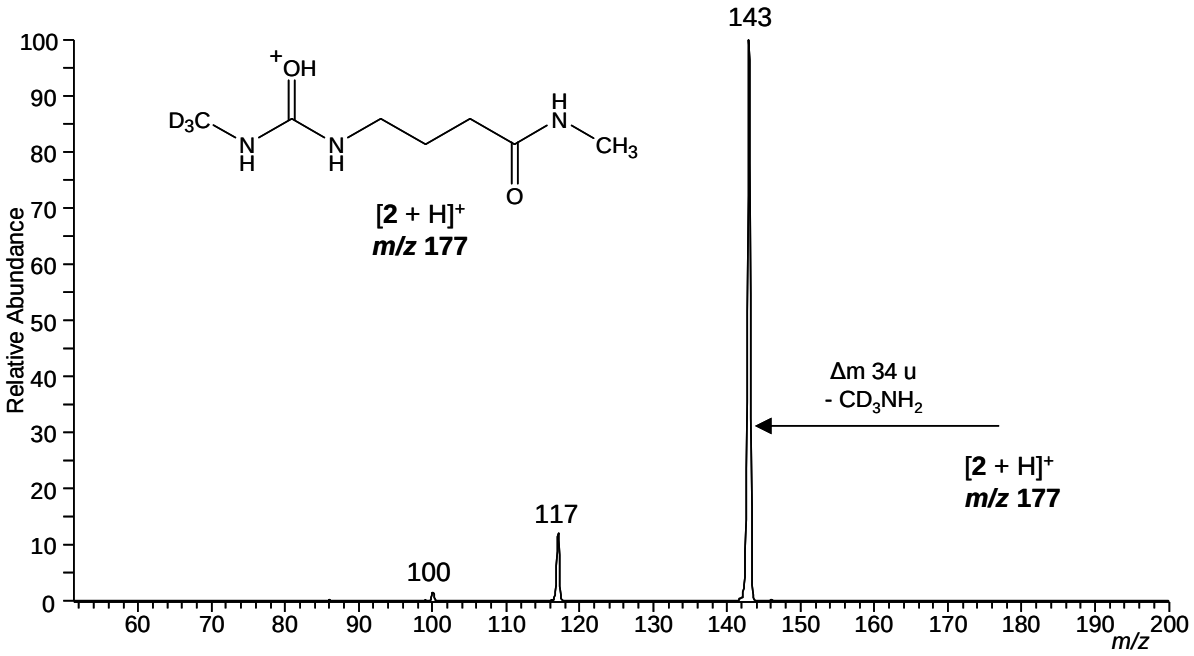


**Figure 3:** ESI-QIT-$MS^2$ product ion spectrum of the protonated precursor ion [**2** + H]$^+$ at *m/z* 177. The precursor ion is completely depleted by CID.

In Figure 3, the ESI-QIT-$MS^2$ product ion spectrum of the protonated molecular ion of **2** is presented. Only the loss of $CD_3NH_2$ and not that of $CH_3NH_2$ is observed (see also Scheme 4). In lower abundance, the trideutero methyl isocyanate is cleaved off to form the ion at *m/z* 117. The minor product ion at *m/z* 100 can again be formed by ammonia loss from *m/z* 117 or directly from the parent ion by loss of methyl urea ($CD_3NHCONH_2$), as Scheme 4 illustrates. Notably, the *m/z* 86 product found in Figure 1 is not observed here, which suggests that this product is *not* formed from *m/z* 117, but rather from *m/z* 162 formed by initial $CH_3NH_2$ loss, the analogue of which is not formed from [**2** + H]$^+$. To rationalize the absence of the loss of $CH_3NH_2$ in the fragmentation pattern of the urea compound **2**, the substantially higher electronegativity of oxygen compared to that of sulphur offers a solution. On this basis, it is reasonable to assume that the ionizing proton is more loosely bound to the thiourea sulphur in the protonated molecular ion of compound **1** than in the urea [**2** + H]$^+$ ion. Consequently, its migration upon CA to less basic sites in the molecule is easier in [**1** + H]$^+$. In the protonated molecular ion [**2** + H]$^+$, the ionizing proton is only transferred to the nitrogens of the urea moiety but not to the amide nitrogen, presumably because of the lower gas-phase basicity of the latter [44, 58], such that the loss of $CH_3NH_2$ is not observed. In addition, the absence of a product ion at *m/z* 146 formed by the loss of $CH_3NH_2$ in the QIT-$MS^2$ spectrum of [**2** + H]$^+$ (see Figure 3) supports the assumption that an acylium ion structure is unlikely for the respective product ion at *m/z* 162 in Figure 1. This is because the formation of the latter should be largely unaffected by the presence of either an urea or a thiourea moiety in the molecule, whereas this substitution should influence formation of the cyclic products.

UU IR Author Manuscript

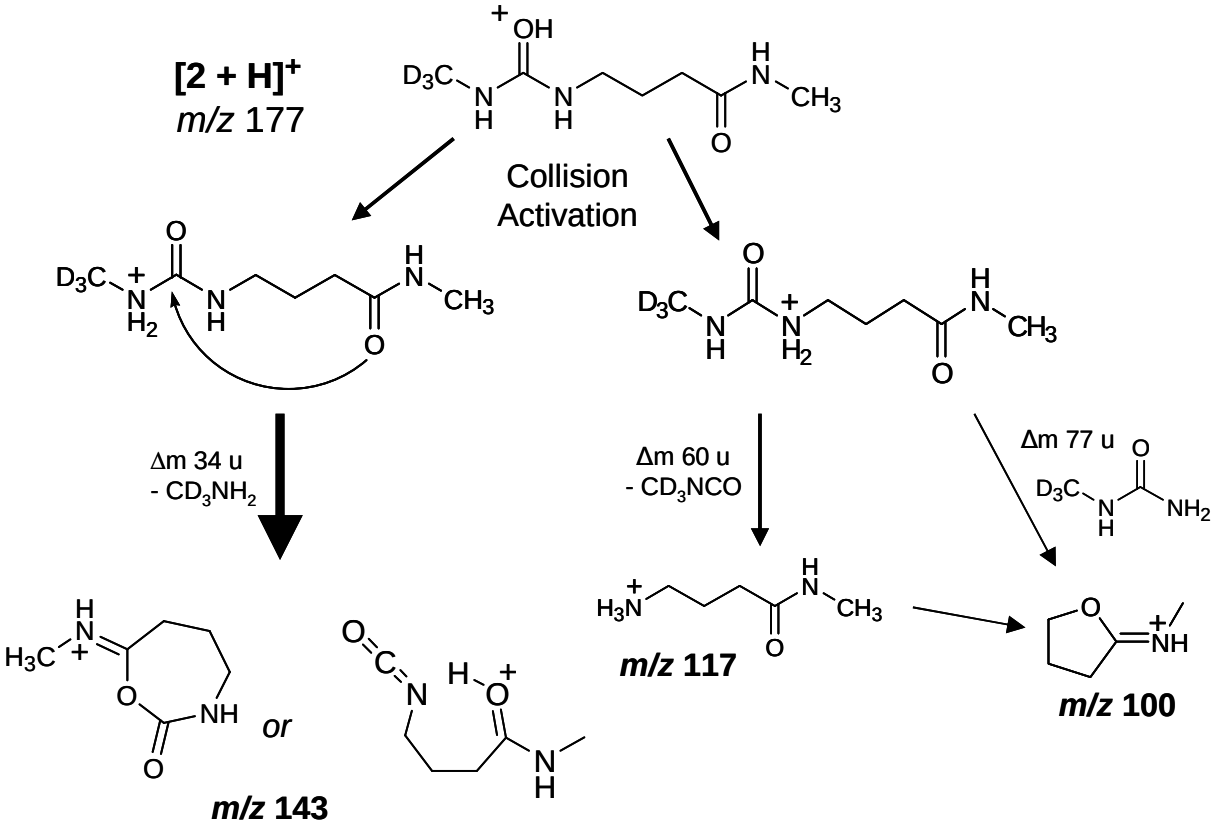


**Scheme 4:** Charge-driven fragmentation pathways observed in the (+)ESI-QIT-MS$^2$ product ion spectrum of the protonated molecular ion [**2** + H]$^+$ at *m/z* 177 (see Figure 3 above).

### 3.1.4. Sodiated molecular ion of compound 2: [2 + Na]$^+$

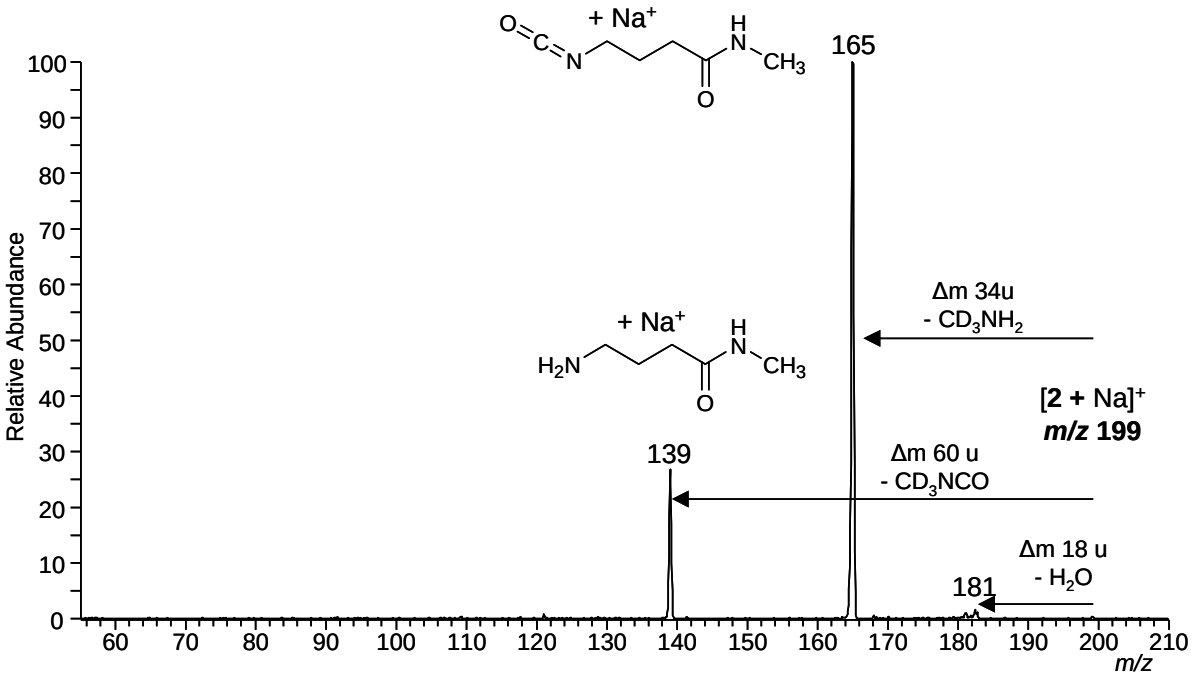


**Figure 4:** ESI-QIT-MS$^2$-product ion spectrum of the sodiated precursor ion [**2** + Na]$^+$ at *m/z* 199. The precursor ion is completely depleted by CID.

In Figure 4, the product ions of the sodiated molecular ion [**2** + Na]$^+$ of compound **2** are presented. The dominant fragmentation channels in the MS$^2$ product ion experiment are related to the formation of alkyl isocyanates, which are either expelled as a neutral (loss of 60u: $CD_3NCO$, product ion *m/z* 139) or remain visible as a sodiated product ion at *m/z* 165 (loss of $CD_3NH_2$). The latter fragmentation reaction is remarkable because the loss of trideutero methylamine $CD_3NH_2$ (Δm 34u) is strongly preferred over the loss of water (*m/z* 181) and the formation of a respective carbodiimide. This striking difference in the fragmentation behavior of the sodiated molecular ions of **1** and **2** can be related to differences in the keto-enol tautomeric equilibrium of the urea- and thiourea-moiety (see Scheme 3). Theoretical and experimental results show that the formation of the enol form is more favored for thiourea-compounds than for respective urea-compounds [64]. On this basis, it seems reasonable to assume that the facilitated loss of hydrogen sulfide observed for [**1** + Na]$^+$, which relies on the proton shift from nitrogen to sulphur, is easier than the analogous loss of water from the sodiated urea compound **2**. In addition, the thermochemistry of the $H_2O$ loss from urea-compounds versus the $H_2S$ loss from thiourea-derivatives strongly favors the former as the C=O bond is much more stable than the C=S bond according to the assumptions of the classical "double bond rule" [65]. Thus, the respective product ion generated by loss of water is hardly visible in Figure 4 (*m/z* 181).

Finally, the higher stability of isocyanates over isothiocyanates reflected in their tautomeric equilibria with corresponding cyanates and thiocyanates, respectively, might also have an influence on the fragmentation patterns of the sodiated molecular ions of **1** and **2** as the formation of alkyl isocyanates is clearly the favored option for compound **2** [66]. These considerations for compound **2** also hold true for the urea-compound **6**, which delivers similar results in MS$^2$ product ion experiments (see SI: Figures 11S - 13S).

### 3.2. Energy-resolved QIT-MS$^2$ product ion experiments of [1 + H]$^+$ and [2 + H]$^+$

Ion activation and CID in QIT-MS is a complex process as it relies on multiple collisions with the He-buffer gas and hence it is difficult to extract quantitative information on the collision energy dependence for selected fragmentation reactions [52]. However, Schröder and others have developed methods to convert phenomenological appearance energies of product ions extracted from experimental QIT-MS breakdown curves into actual critical energies of fragmentation reactions [25, 26, 30, 67, 68]. In the case of the spherical QIT-MS Esquire 3000 plus by *Bruker Daltonics* in which the MS$^2$ product ion experiments were conducted, the amplitude of the RF-voltage used for excitation is controlled experimentally. This rather abstract value can be transformed to estimated threshold energies of certain fragmentation reactions in relation to well described fragmentation reactions of so called thermometer ions with well documented threshold energies, e.g., fragmentation reactions of substituted benzylpyridinium ions as suggested by DePauw and others [67, 69-73]. However, it must be stressed that the energy-resolved product ion experiments in QIT-MS yield only rough estimates as the CID process and the internal energy distribution of the precursor ion is ill defined [25]. Threshold CID experiments on guided-ion-beam-instruments with much better control of the experimental conditions defining the source and individual collision events combined with accurate data evaluation [74-76] are underway to determine correct absolute threshold energies for the fragmentation reactions of interest here. Even though *absolute* critical energies deduced from QIT-MS are unreliable, *relative* QIT-MS

UU IR Author Manuscript

threshold values of competing fragmentation reactions are less compromised by the experimental uncertainties and provide useful energetic information [30].

In the present work, threshold activation voltages are determined with mass-selected precursor ions by gradually increasing the activation voltage until complete depletion of the precursor ion is observed. In doing so, a breakdown curve with a sigmoidal shape is obtained from which the threshold voltage can either be determined as the voltage at which the fragment ion intensity has reached a certain percentage of the total ion intensity (e.g., 5% [30], 10% [29], or 50% [28]) or be determined by linear extrapolation of the slope of the breakdown curve to the baseline [25]. The latter procedure is utilized here, where the data analyzed include the most linear region of the rising curve.

Energy-dependent dissociation studies of compounds **1** and **2** yielded the breakdown curves shown in Figures 5 and 6. Linear extrapolation of the product ion curves of interest, i.e., product ions at *m/z* 159 and *m/z* 162 in Figure 5 and of product ion at *m/z* 143 in Figure 6, lead to nearly equal threshold voltages of 0.11 – 0.12 V. We estimate an experimental error of at least 10 % by judging the quality of the linear fit and the deviations of ion abundances measured. However, the similar appearance energies of all three product ions lead to the following hypotheses:

1) As strongly different product ion yields of the competing fragmentation reactions are found (see Figure 1), the two reaction channels (i.e., the loss of $CD_3NH_2$ vs. $CH_3NH_2$ leading to the formation of product ions at *m/z* 159 and *m/z* 162; Figure 1) proceed via different mechanisms including different entropic demands of the transition state (TS), which in turn suggests different product ion structures. For the [**1** + H]$^+$ ion, this assumption strongly points towards the formation of one of the heterocyclic product ions at *m/z* 162 found as result of the nucleophilic attack of the thiourea-sulphur or urea nitrogen onto the adjacent amide bond and the protonated isothiocyanate structure for the ion at *m/z* 159 (see Scheme 2). As similar appearance energies are found for the fragment ion of [**2** + H]$^+$ at *m/z* 143 and the respective fragment ion generated from [**1** + H]$^+$at *m/z* 159, both corresponding to loss of $CD_3NH_2$, a nucleophilic attack of the amide oxygen onto either the urea carbonyl in the former and the attack on the thiocarbonyl in the latter is unlikely because the double bond of the thiocarbonyl-moiety in **1** is much less polarized than the carbonyl moiety in **2**. This conclusion also points towards the open chain protonated isocyanate structure of the product ion at *m/z* 143 and the analogous isothiocyanate structure for the ion at *m/z* 159.

2) The rate-determining steps are migrations of the ionizing proton upon CA, which precedes dissociation events of the protonated molecular ions of compound **1** and **2**. Hence, the appearance energies taken from the QIT-MS$^2$ breakdown curves correspond to these transition states and therefore may not provide any information on the actual fragmentation pathways and the respective reaction mechanisms of the precursor ions examined in the QIT-MS$^2$ experiments.

These assumptions and hypotheses are now probed in more detail by theory.

UU IR Author Manuscript

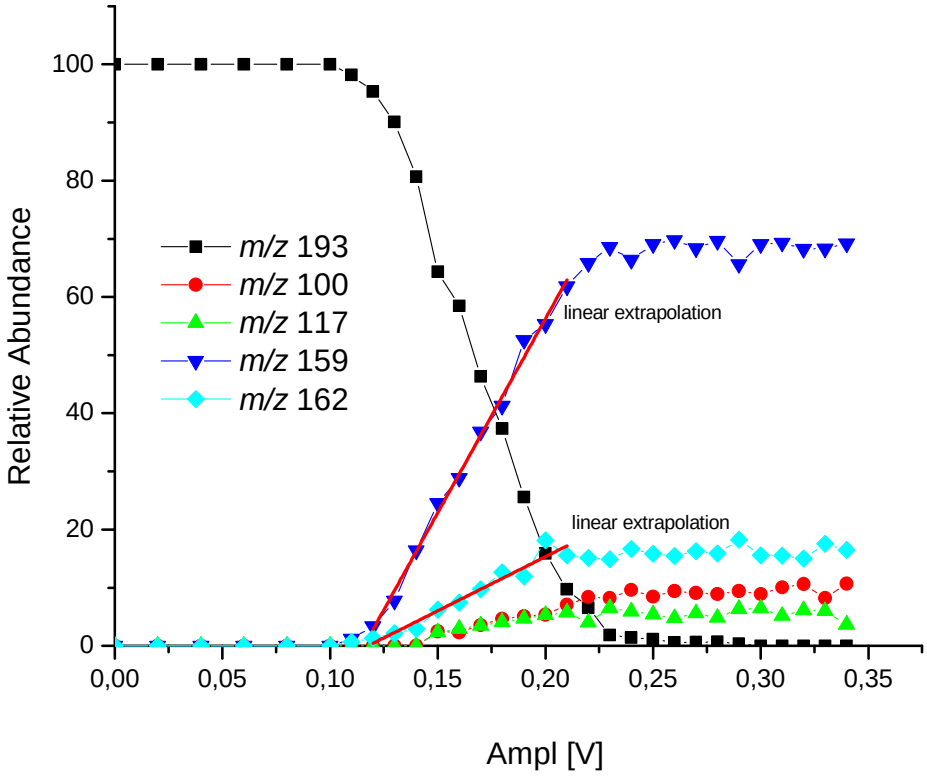


**Figure 5:** Energy resolved (+)ESI-QIT-$MS^2$ product ion experiments of the protonated molecular ion $[\mathbf{1} + H]^+$ of compound **1** (precursor ion *m/z* 193). (Linear regression analyses using data points from 0.12 - 0.21 V: ***m/z* 159:** y = 667.3·x - 77.2; $R^2$ = 0.99; ***m/z* 162:** y = 186.1·x - 21.9; $R^2$ = 0.94).

UU IR Author Manuscript

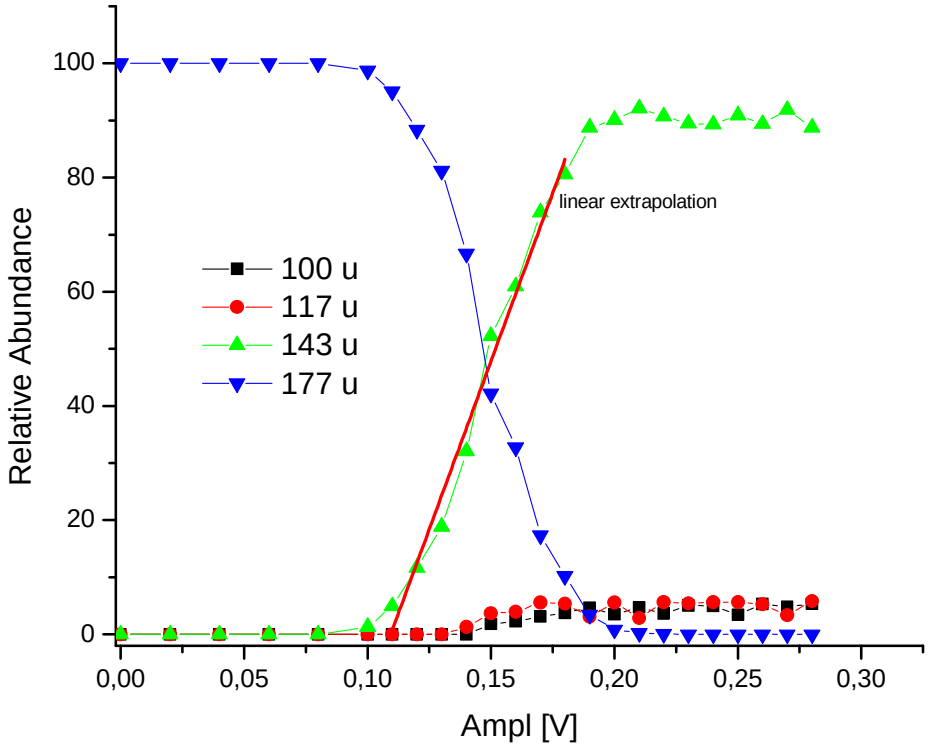


**Figure 6:** Energy resolved (+)ESI-QIT-$MS^2$ product ion experiments of the protonated molecular ion [**2** + H]$^+$ of compound **2** (precursor ion *m/z* 177). (Linear regression analysis using data points from 0.11 - 0.18 V: **m/z 143:** y = 1176.9·x - 128.7; $R^2$ = 0.98).

### 3.3. Computational analysis of the reaction pathways

To further elucidate the fragmentation pathways and to probe the assumptions drawn on the basis of the QIT-$MS^2$ data set, the CID behavior of the protonated molecular ions of **1** and **2** were closely examined by theory. Careful scans of the PES yield characteristic transition states for loss of $CD_3NH_2$, Schemes 5 and 6. In both schemes, the first step takes the ground state conformation and rotates the (thio) urea group around a CN bond to form a higher energy conformer of the protonated molecular ions. Then the proton is transferred from the S or O in the (thio) urea group to the nitrogen adjacent to the labelled methyl group. The N-protonated intermediates formed can then lose $CD_3NH_2$ readily by simple bond cleavage to yield the protonated isothiocyanate structure of product ion *m/z* 159 of [**1** + H]$^+$ and the respective isocyanate structure for the ion at *m/z* 143 of [**2** + H]$^+$. At higher energies, nucleophilic attack of the carbonyl oxygen at the urea carbon can form the seven-membered ring forms of the two product ions. These heterocyclic structures are higher in energy by 49 – 63 kJ/mol for [**1**+H]$^+$ and 14 – 24 kJ/mol for [**2**+H]$^+$ and therefore less likely to be formed. Indeed, the energy of the heterocyclic product greatly exceeds that of the rate-limiting TS in the thiourea case, whereas it is energetically accessible for the urea case.

An important conclusion from these schemes is that the migration of the ionizing proton along the molecule backbone, which takes place upon collision activation prior to fragmentation, is the rate-limiting step that determines the extent of the charge driven fragmentation processes that follow for both reactant ions. Furthermore, theory finds they

have comparable energy barriers: 138 – 145 kJ/mol for **1** and 154 – 159 kJ/mol for **2** (see Schemes 5 and 6). The predicted critical energies for the migration of the ionizing proton differ by about 10%, which is in good agreement with the outcome of the energy resolved QIT-$MS^2$ studies of the protonated molecular ions of **1** and **2**.

Scheme 7 shows the computed pathway for formation of the product ion at *m/z* 162 from protonated **1**. The first step is proton transfer from the sulphur to the nitrogen followed by nucleophilic attack of the sulphur at the carbonyl carbon, which induces loss of $CH_3NH_2$. For protonated compound **2,** the analogous pathway to Scheme 7 was also explored by using potential energy surface scans. Here, no stable intermediates could be located anywhere along the surface, which agrees well with experiment as the loss of $CH_3NH_2$ is not found in QIT-$MS^2$ of compound **2** (see Figure 3). This finding certainly goes back to the fact that the urea carbonyl oxygen of compound **2** is substantially less nucleophilic than the respective sulphur of compound **1**. Oxygen is substantially more electronegative than sulphur, and thus the oxygen binds the ionizing proton more tightly, thereby effectively restricting the mobility of that proton. Theoretically, the product ion at *m/z* 162 found in the $MS^2$ spectrum of $[\mathbf{1} + H]^+$ is suggested to be a 7-membered heterocyclic ion structure, whereas the alternative γ-butyrolactame derivative structure is 38 – 60 kJ/mol higher and the acylium ion structure (formed by simple CN bond cleavage) lies 79 - 85 kJ/mol higher in energy. In this process, the products limit the overall energy for $CH_3NH_2$ elimination, lying 136 – 146 kJ/mol above the GS reactant, whereas the TS for proton transfer along this PES lies 12 – 46 kJ/mol lower in energy, Scheme 7. This critical energy is nearly identical with that predicted for $CD_3NH_2$ loss, which also agrees well with experiment as the energy resolved QIT-$MS^2$ studies yield similar thresholds for $CH_3NH_2$ and $CD_3NH_2$ losses, Figure 5. Given the similar energetics, it appears that the former process is disfavored because its proton transfer requires formation of a 9-membered cyclic TS and cyclization of the products, whereas the latter process utilizes a 7-membered cyclic TS and forms the more open isothiocyanate.

Finally, the theoretical approach used here has located a reasonable pathway for decomposition of the parent ions to lose $CD_3NHCXNH_2$ (X = S or O) and of the *m/z* 117 product to lose ammonia yielding *m/z* 100. The formation of the *m/z* 86 product ion is still being investigated, but the most likely pathway appears to be nucleophilic attack of the thiourea nitrogen of protonated **1** at the carbonyl, displacing $CH_3NH_2$ and forming the γ-butyrolactame derivative isomer of the *m/z* 162 product ion, which then easily loses $CD_3NCS$.

UU IR Author Manuscript

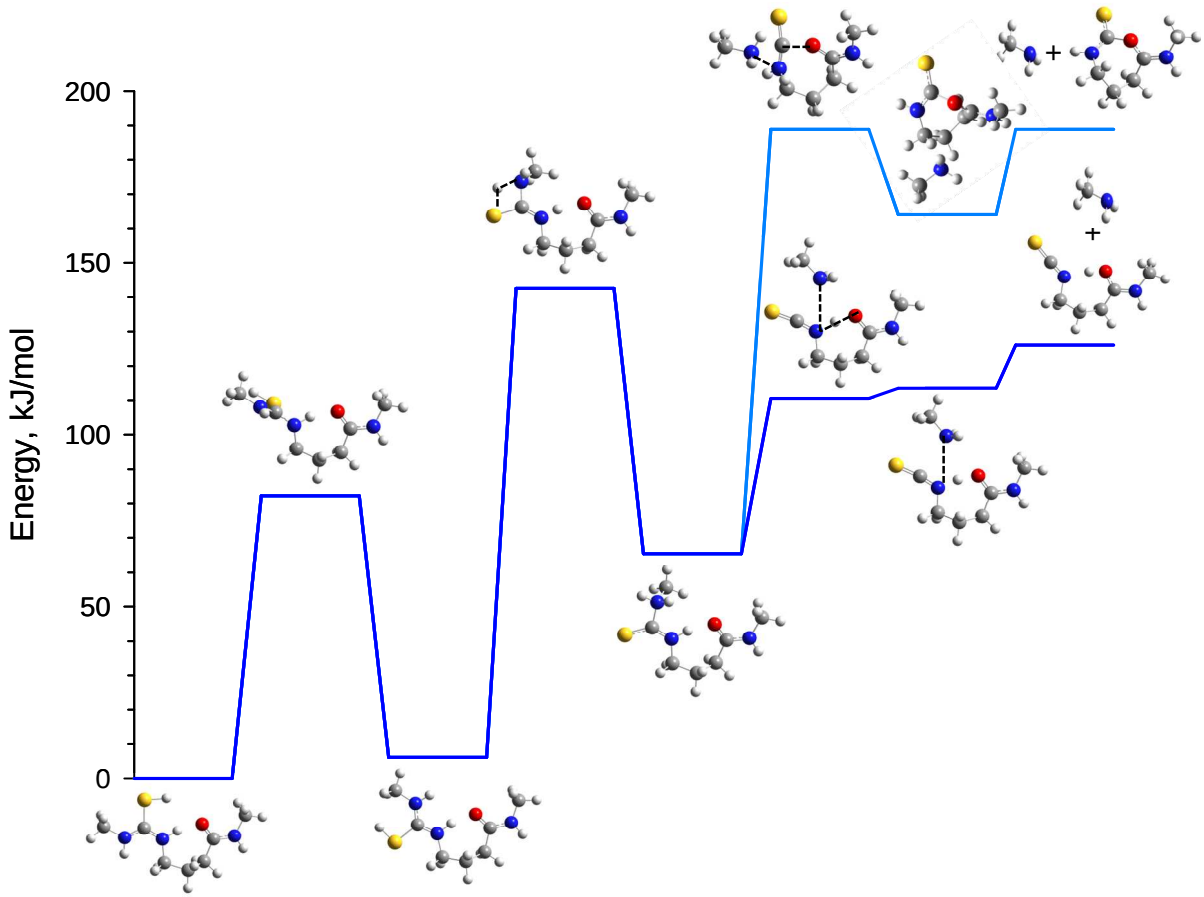


**Scheme 5:** Computed reaction pathway of the migration of the ionizing proton from the most basic site in the molecular ion [**1** + H]$^+$ upon CA to the adjacent thiourea nitrogen followed by dissociation to products at *m/z* 159. Dashed lines indicate bonds being broken or formed. Only key steps are shown.

UU IR Author Manuscript

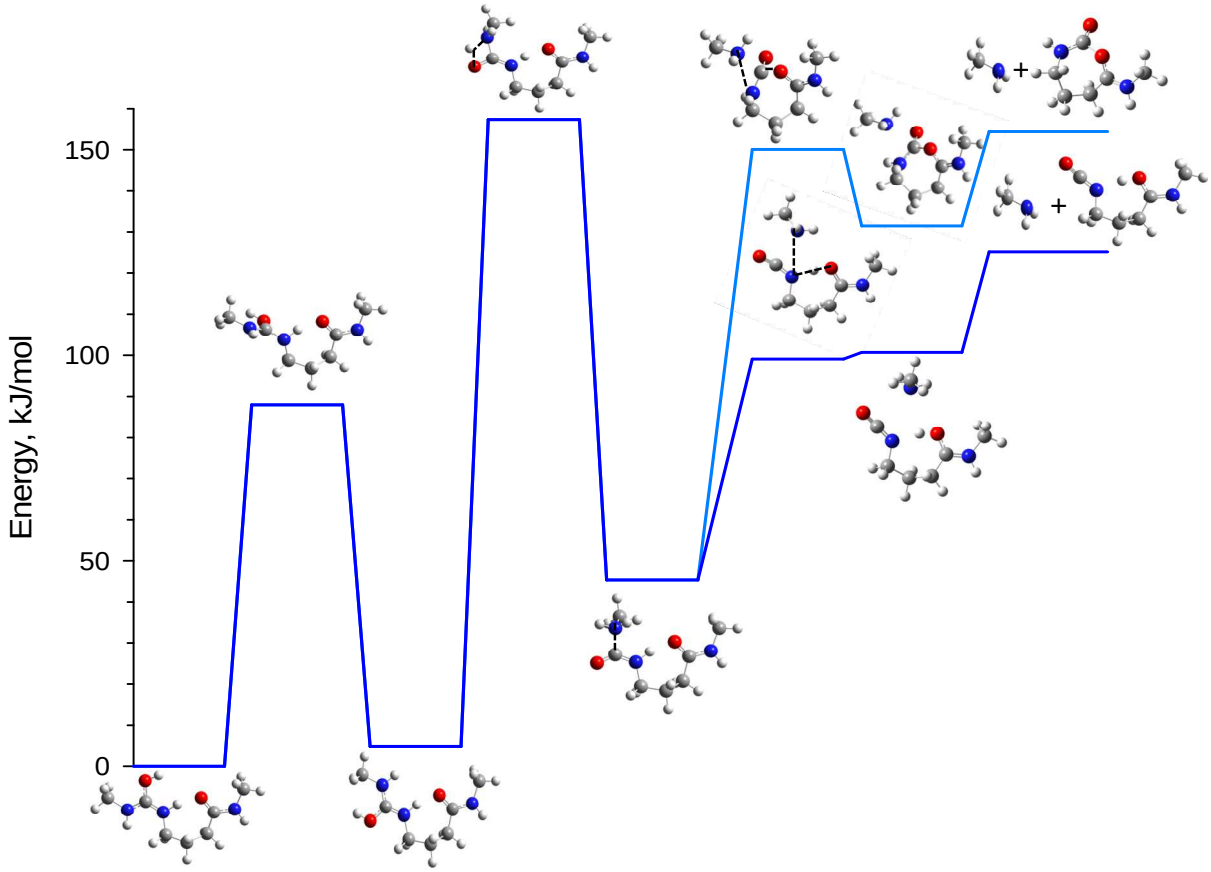


**Scheme 6:** Computed reaction pathway of the migration of the ionizing proton from the most basic site in the molecular ion [**2** + H]$^+$ upon CA to the adjacent urea nitrogen followed by dissociation to products at *m/z* 143. Dashed lines indicate bonds being broken or formed. Only key steps are shown.

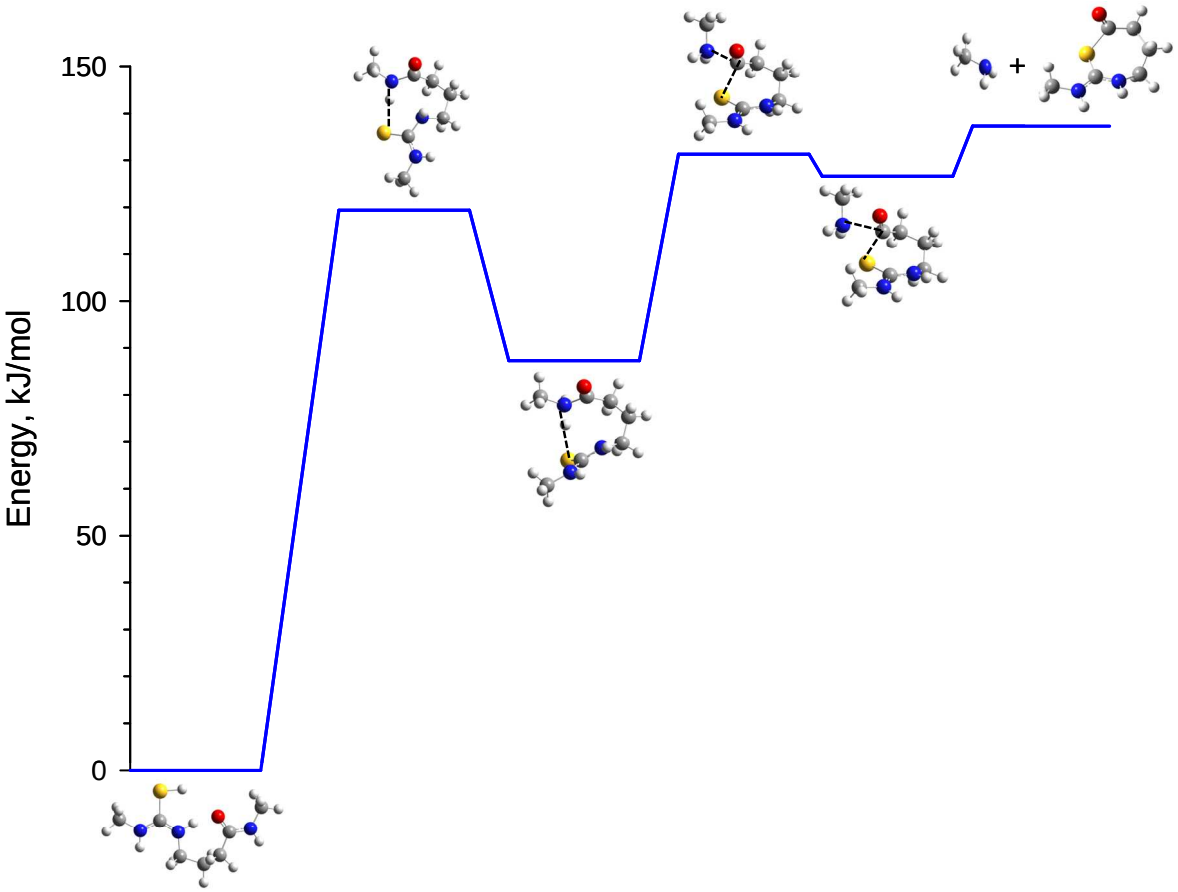


**Scheme 7:** Computed reaction pathway of the migration of the ionizing proton from the most basic site in the molecular ion [**1** + H]$^+$ upon CA to the amide nitrogen followed by dissociation to products at *m/z* 162. Dashed lines indicate bonds being broken or formed. Only key steps are shown.



## 4. Conclusions

Results of the QIT-MS$^2$-experiments document the subtle competition of the fragmentation pathways of the set of structurally related urea and thiourea-compounds. The extensive examination of the fragmentation behavior demonstrates that the substitution of sulphur for oxygen in the urea moiety influences the fragmentation pattern. Additionally, these results stress the vital importance of the urea moiety on the fragmentation pathways and the effective functioning of urea-reagents as CID-labile XL-compounds. However, it is noted that the model-compounds with thiourea-moieties examined in this study differ from the characteristic fragmentation behavior found for the actual thiourea-XL-compounds. The reason for this deviation is not yet fully understood and is currently being investigated by theory and additional tandem-MS experiments with other tailor made compounds.

The energy-dependent dissociation experiments conducted in a spherical QIT yield comparable if not equal threshold energies for the major competing fragmentation reactions under investigation. The characteristic fragmentation reactions of the set of precursor ions lead to product ions for which different isomeric structures are considered, i.e., 7-membered heterocyclic ring, a γ-butyrolactame-derivative, or open chain isothiocyanate and isocyanate ion structures. Theoretical PESs and the extensive set of experimental results provide a consistent picture of the results, which allows a reliable identification of individual ion

structures. More advanced energetic experiments remain desirable in order to allow a more quantitative comparison of the computational results with experiments.

The computational analysis of the fragmentation pathways by careful scans of the PES yield characteristic transition states strongly suggesting that the migration of the ionizing proton along the molecule backbone, which takes place upon collision activation prior to fragmentation, is the rate-limiting step for the dominant fragmentation pathways. The computations clearly show that the initial transition state of the respective proton moving from the most basic site of the precursor ion (the thiourea-sulphur in **1** and the urea carbonyl oxygen in **2**) to less basic heteroatom sites of the molecule is the necessary and decisive step that determines the extent of the charge-driven fragmentation processes that follow. This step determines the overall energetics of the major fragmentation processes.

**Acknowledgments**

This work is generously supported by a doctoral fellowship of the "Cusanuswerk" to L.F. and by financial support by the DFG to M.S., F.D. and F.F. which is gratefully acknowledged. M.S., L.F., and F.F. thank Prof. Klaus Meerholz (Department of Chemistry, Institute of Physical Chemistry, University of Cologne) for allowing us to use the *Bruker Daltonics* Esquire 3000 plus QIT-MS instrument for the series of energy-resolved $MS^2$ experiments. R.W. and P.B.A. thank the National Science Foundation, Grant No. CHE-1049580, for support and the Center for High Performance Computing at the University of Utah for the generous allocation of computer time.

Supplementary information (SI) associated with this article can be found, in the online version, at **doi:XXXXX**.

**References**

[1] A. Sinz, Angew. Chem. Int. Ed. 46 (2007) 660.
[2] A. Sinz, J. Mass Spectrom. 38 (2003) 1225.
[3] A. Sinz, Mass Spectrom. Rev. 25 (2006) 663.
[4] M.A. Trakselis, S.C. Alley, F.T. Ishmael, Biocon. Chem. 16 (2005) 741.
[5] F. Dreiocker, M.Q. Müller, A. Sinz, M. Schäfer, J. Mass Spectrom. 45 (2010) 178.
[6] M.Q. Müller, F. Dreiocker, C.H. Ihling, M. Schäfer, A. Sinz, J. Mass Spectrom. 45 (2010) 880.
[7] M.Q. Müller, J.J. Zeiser, F. Dreiocker, A. Pich, M. Schäfer, A. Sinz, Rapid Commun. Mass Spectrom. 25 (2011) 155.
[8] E.J. Soderblom, M.B. Goshe, Anal. Chem. 78 (2006) 8059.
[9] A. Kao, C. Chiu, D. Vellucci, Y. Yang, V.R. Patel, S. Guan, A. Randall, P. Baldi, S.D. D. Rychnovsky, L. Huang, Mol. Cell. Prot. 10 (2011).
[10] S.M. Chowdhury, G.R. Munske, X.T. Tang, J.E. Bruce, Anal. Chem. 78 (2006) 8183.
[11] M.Q. Müller, F. Dreiocker, C.H. Ihling, M. Schäfer, A. Sinz, Anal. Chem. 82 (2010) 6958.
[12] F. Falvo, F. Dreiocker, M. Schäfer, in: Proceedings of the 44th Conference of the German Mass Spectrometry Society DGMS, Dortmund, 2011.
[13] F. Falvo, L. Fiebig, F. Dreiocker, M. Schäfer, in: Proceedings of the 45th Conference of the German Mass Spectrometry Society, Poznan, 2012.
[14] S.G. Summerfield, H. Steen, M. O'Malley, S.J. Gaskell, Int. J. Mass Spectrom. 188 (1999) 95.
[15] B.T. Chait, R. Wang, R.C. Beavis, S.B.H. Kent, Science, 262 (1993) 89.
[16] R. Wang, B.T. Chait, Protein Ladder Sequencing, in: J.M. Walker (Ed.) The Protein Protocols Handbook, Humana Press. Inc., Totowa New Jersey, 2002, pp. 733.
[17] A. Berkessel, S. Mukherjee, T.N. Muller, F. Cleemann, K. Roland, M. Brandenburg, J.M. Neudörfl, J. Lex, Org. Biomol. Chem. 4 (2006) 4319.

UU IR Author Manuscript

[18] A. Berkessel, K. Roland, J.M. Neudörfl, Org. Lett. 8 (2006) 4195.
[19] R.R. Knowles, S. Lin, E.N. Jacobsen, J. Am. Chem. Soc. 132 (2010) 5030.
[20] E.A. Peterson, E.N. Jacobsen, Angew. Chem.Int. Ed. 48 (2009) 6328.
[21] S.J. Connon, Chem. Eur. J. 12 (2006) 5418.
[22] Y. Takemoto, Org. Biomol. Chem. 3 (2005) 4299.
[23] P. Perez, C. Simo, C. Neususs, M. Pelzing, J. San Roman, A. Cifuentes, A. Gallardo, Biomacromol. 7 (2006) 720.
[24] J.M. Berg, J.L. Tymoczko, L. Stryer, Biochemistry, 5th Ed, in, Palgrave MacMillan, New York, 2002.
[25] E.L. Zins, C. Pepe, D. Schröder, J. Mass Spectrom. 45 (2010) 1253.
[26] Á. Rèvèsz, C. Milko, J. Žabka, D. Schröder, J. Mass Spectrom. 45 (2010) 1246.
[27] J. Chen, Y. Lu, L. Lin, Z. Sun, C. Sun, Y. Pan, Rapid Commun. Mass Spectrom. 23 (2009) 1654.
[28] N. Vinokur, V. Ryzhov, J. Mass Spectrom. 39 (2004) 1268.
[29] T. Waters, R.A.J. O'Hair, A.G. Wedd, J. Am. Chem. Soc. 125 (2003) 3384.
[30] J.M. Zhang, J.S. Brodbelt, J. Am. Soc. Mass Spectrom. 16 (2005) 139.
[31] R. Castonguay, C. Lherbet, J.W. Keillor, Bioorgan. Med. Chem. 10 (2002) 4185.
[32] http://www.archimica.com/PDF/ARCHIMICA_T3P_Brochure.pdf.
[33] M.L. Moore, F.S. Crossley, Org. Synth. 3 (1955) 599.
[34] J. Kalm, Contribution from the chemical Research Division of G. Searle & Co., (1960) 2925.
[35] D.A. Pearlman, D.A. Case, J.W. Caldwell, W.R. Ross, T.E. Cheatham, S. DeBolt, D. Ferguson, G. Seibel, P. Kollman, Comp. Phys. Commun. 91 (1995) 1.
[36] E.J. Bylaska, W.A. deJong, K. Kowalski, T.P. Straatsma, M. Valiev, D. Wang, E. Aprà, T.L. Windus, S. Hirata, M.T. Hackler, Y. Zhao, P.-D. Fan, R.J. Harrison, M. Dupuis, D.M.A. Smith, J. Nieplocha, V. Tipparaju, M. Krishnan, A.A. Auer, M. Nooijen, E. Brown, G. Cisneros, G.I. Fann, H. Früchtl, J. Garza, K. Hirao, R. Kendall, J.A. Nichols, K. Tsemekhman, K. Wolinski, J. Anchell, D. Bernholdt, P. Borowski, T. Clark, D. Clerc, H. Dachsel, M. Deegan, K. Dyall, D. Elwood, E. Glendening, M. Gutowski, A. Hess, J. Jaffe, B. Johnson, J. Ju, R. Kobayashi, R. Kutteh, Z. Lin, R. Littlefield, X. Long, B. Meng, T. Nakajima, S. Niu, L. Pollack, M. Rosing, G. Sandrone, M. Stave, H. Taylor, G. Thomas, J.v. Lenthe, A. Wong, Z. Zhang, NWChem, A Computational Chemistry Package for Parallel Computers. Pacific Northwest National Laboratory, Richland, Washington 99352, (2003).
[37] C.C. Roothaan, Rev. Mod. Phys. 23 (1951) 69.
[38] J.S. Binkley, J.A. Pople, W.J. Hehre, J. Am. Chem. Soc. 102 (1980) 939.
[39] M.J. Frisch, G.W. Trucks, H.B. Schlegel, G.E. Scuseria, M.A. Robb, J.R. Cheeseman, G. Scalmani, V. Barone, B. Mennucci, G.A. Petersson, H. Nakatsuji, M. Caricato, X. Li, H.P. Hratchian, A.F. Izmaylov, J. Bloino, G. Zheng, J.L. Sonnenberg, M. Hada, M. Ehara, K. Toyota, R. Fukuda, J. Hasegawa, M. Ishida, T. Nakajima, Y. Honda, O. Kitao, H. Nakai, T. Vreven, J. Montgomery, J. A., J.E. Peralta, F. Ogliaro, M. Bearpark, J.J. Heyd, E. Brothers, K.N. Kudin, V.N. Staroverov, R. Kobayashi, J. Normand, K. Raghavachari, A. Rendell, J.C. Burant, J.M. Millam, S.S. Iyengar, J. Tomasi, M. Cossi, N. Rega, J.M. Millam, M. Klene, J.E. Knox, J.B. Cross, V. Bakken, C. Adamo, J. Jaramillo, R. Gomperts, R.E. Stratmann, O. Yazyev, A.J. Austin, R. Cammi, C. Pomelli, J.W. Ochterski, R.L. Martin, K. Morokuma, V.G. Zakrzewski, G.A. Voth, P. Salvador, J.J. Dannenberg, S. Dapprich, A.D. Daniels, O. Farkas, J.B. Foresman, J.V. Ortiz, J. Cioslowski, D.J. Fox, Gaussian Inc.: Pittsburgh, PA, (2009).
[40] A.D. Becke, J. Chem. Phys., 98 (1993) 5648.
[41] R. Ditchfield, W.J. Hehre, J.A. Pople, J. Chem. Phys. 54 (1971) 724.
[42] A.D. McLean, G.S. Chandler, J. Chem. Phys. 72 (1980) 5639.
[43] J.B. Foresman, A.E. Frisch, Exploring Chemistry with Electronic Structure Methods, Gaussian, Inc., Pittsburgh, PA, 1996.
[44] B. Paizs, S. Suhai, Mass Spectrom. Rev. 24 (2005) 508.
[45] B. Paizs, S. Suhai, J. Am. Soc. Mass Spectrom. 15 (2004) 103.
[46] P.B. Armentrout, A.L. Heaton, J. Am. Soc. Mass Spectrom. 23 (2012) 621.
[47] P.B. Armentrout, A.L. Heaton, J. Am. Soc. Mass Spectrom. 23 (2012) 632.
[48] P. Roepstorff, J. Fohlman, Biomed. Mass Spectrom. 11 (1984) 601.

[49] T. Yalcin, C. Khouw, I.G. Csizmadia, M.R. Peterson, A.G. Harrison, J. Am. Soc. Mass Spectrom. 6 (1995) 1165.
[50] S.A. McLuckey, D.E. Groeninger, J. Mass. Spectrom. 32 (1997) 461.
[51] M.W. Senko, J.B. Cunniff, A.P. Land, in: Proceedings of the 46th ASMS Conference on Mass Spectrometry and Allied Topics, Orlando, Fl, 1998, p. 486.
[52] R.E. March, Ion Traps, in: M.L. Gross, R. Caprioli (Eds.) Encyclopedia of Mass Spectrometry, Elsevier, San Diego, 2004, pp. 144.
[53] R.E. March, J. Mass Spectrom. 32 (1997) 351.
[54] R.G. Cooks, R.E. Kaiser, Acc. Chem. Res. 23 (1990) 213.
[55] V.H. Wysocki, H.I. Kenttamaa, R.G. Cooks, Int. J. Mass Spectrom. Ion Proc. 75 (1987) 181.
[56] V.H. Wysocki, G. Tsaprailis, L.L. Smith, L.A. Breci, J. Mass Spectrom. 35 (2000) 1399.
[57] K. Biemann, Mass Spectrom. Rev. 6 (1987) 1.
[58] A.R. Dongre, J.L. Jones, A. Somogyi, V.H. Wysocki, J. Am. Chem. Soc. 118 (1996) 8365.
[59] S.G. Summerfield, A. Whiting, S.J. Gaskell, Int. J. Mass Spectrom. Ion Proc. 162 (1997) 149.
[60] O. Burlet, R.S. Orkiszewski, K.D. Ballard, S.J. Gaskell, Rapid Commun. Mass Spectrom. 6 (1992) 658.
[61] A.G. Harrison, T. Yalcin, Int. J. Mass Spectrom. 165 (1997) 339.
[62] R.S. Johnson, D. Krylov, K.A. Walsh, J. Mass Spectrom. 30 (1995) 386.
[63] K.A. Cox, S.J. Gaskell, M. Morris, A. Whiting, J. Am. Soc. Mass Spectrom. 7 (1996) 522.
[64] P.E. Allegretti, E.A. Castro, J.J.P. Furlong, J. Mol. Struc.-Theochem. 499 (2000) 121.
[65] P. Jutzi, Angew. Chem. Int. Ed. 14 (1975) 232.
[66] M.B. Smith, J. March, March's Advanced Organic Chemistry: Reactions, Mechanisms, and Structure 6th Ed., John Wiley & Sons, New York (2007).
[67] E.L. Zins, D. Rondeau, P. Karoyan, C. Fosse, S. Rochut, C. Pepe, J. Mass Spectrom. 44 (2009) 1668.
[68] E.L. Zins, C. Pepe, D. Rondeau, S. Rochut, N. Galland, J.C. Tabet, J. Mass Spectrom. 44 (2009) 12.
[69] K.V. Barylyuk, K. Chingin, R.M. Balabin, R. Zenobi, J. Am. Soc. Mass Spectrom. 21 (2010) 172.
[70] V. Gabelica, E. De Pauw, Mass Spectrom. Rev. 24 (2005) 566.
[71] J. Naban-Maillet, D. Lesage, A. Bossee, Y. Gimbert, J. Sztaray, K. Vekey, J.C. Tabet, J. Mass Spectrom. 40 (2005) 1.
[72] J.F. Greisch, V. Gabelica, F. Remacle, E. De Pauw, Rapid Commun. Mass Spectrom. 17 (2003) 1847.
[73] C. Collette, E. De Pauw, Rapid Commun. Mass Spectrom. 12 (1998) 165.
[74] P.B. Armentrout, K.M. Ervin, M.T. Rodgers, J. Phys. Chem. A 112 (2008) 10071.
[75] K.M. Ervin, Chem. Rev. 101 (2001) 391.
[76] P.B. Armentrout, Int. J. Mass Spectrom. 200 (2000) 219.

# Fragmentation reactions of thiourea- and urea-compounds examined by tandem MS-, energy-resolved CID experiments, and theory

Francesco Falvo, Lukas Fiebig, Frank Dreiocker, Ran Wang,
P. B. Armentrout and **Mathias Schäfer**

## Supporting Information

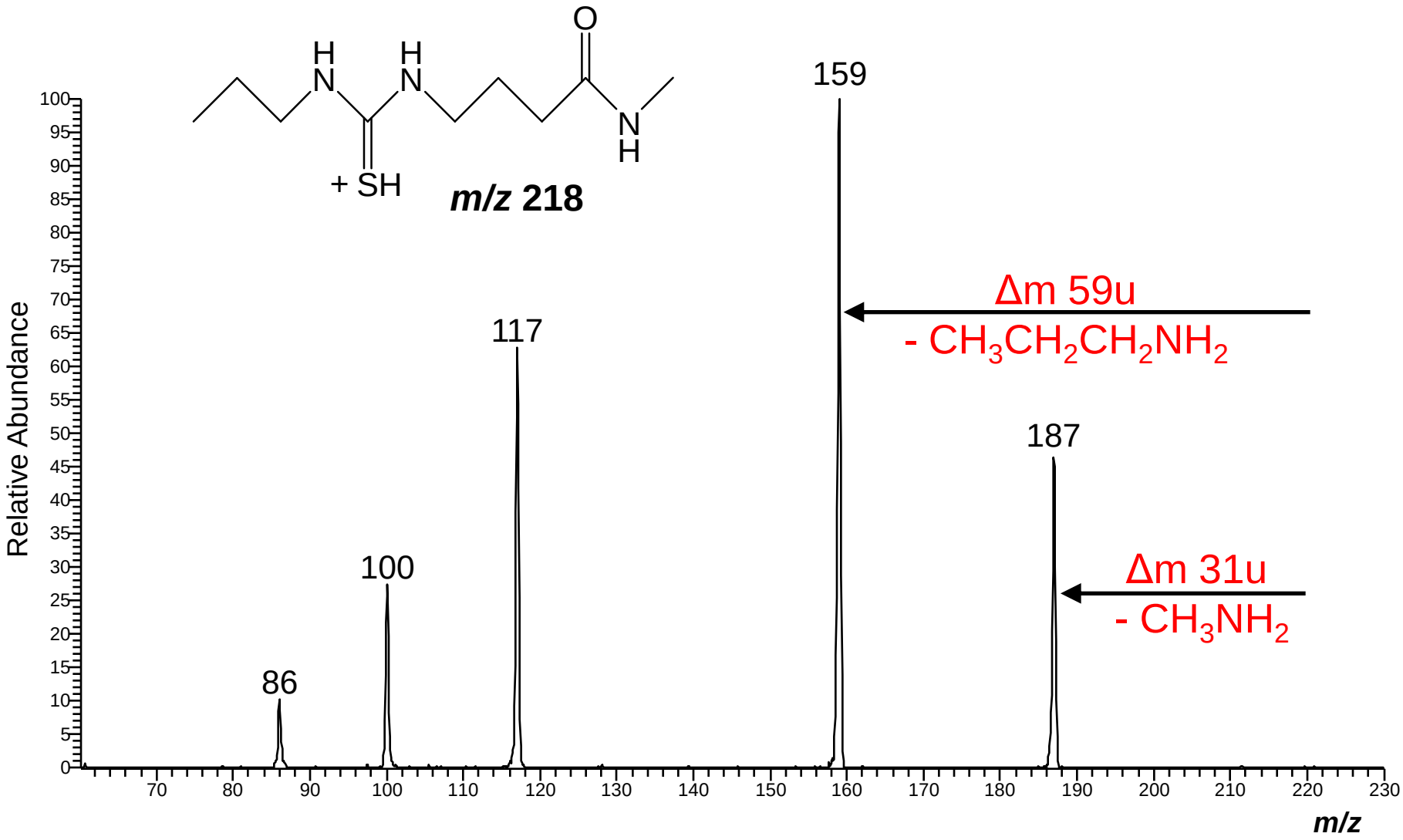


**Figure 1S:** (+)ESI-QIT-MS$^2$ product ion spectrum of the protonated precursor ion [**3** + H]$^+$ at *m/z* 218. The precursor ion is completely depleted by CID.

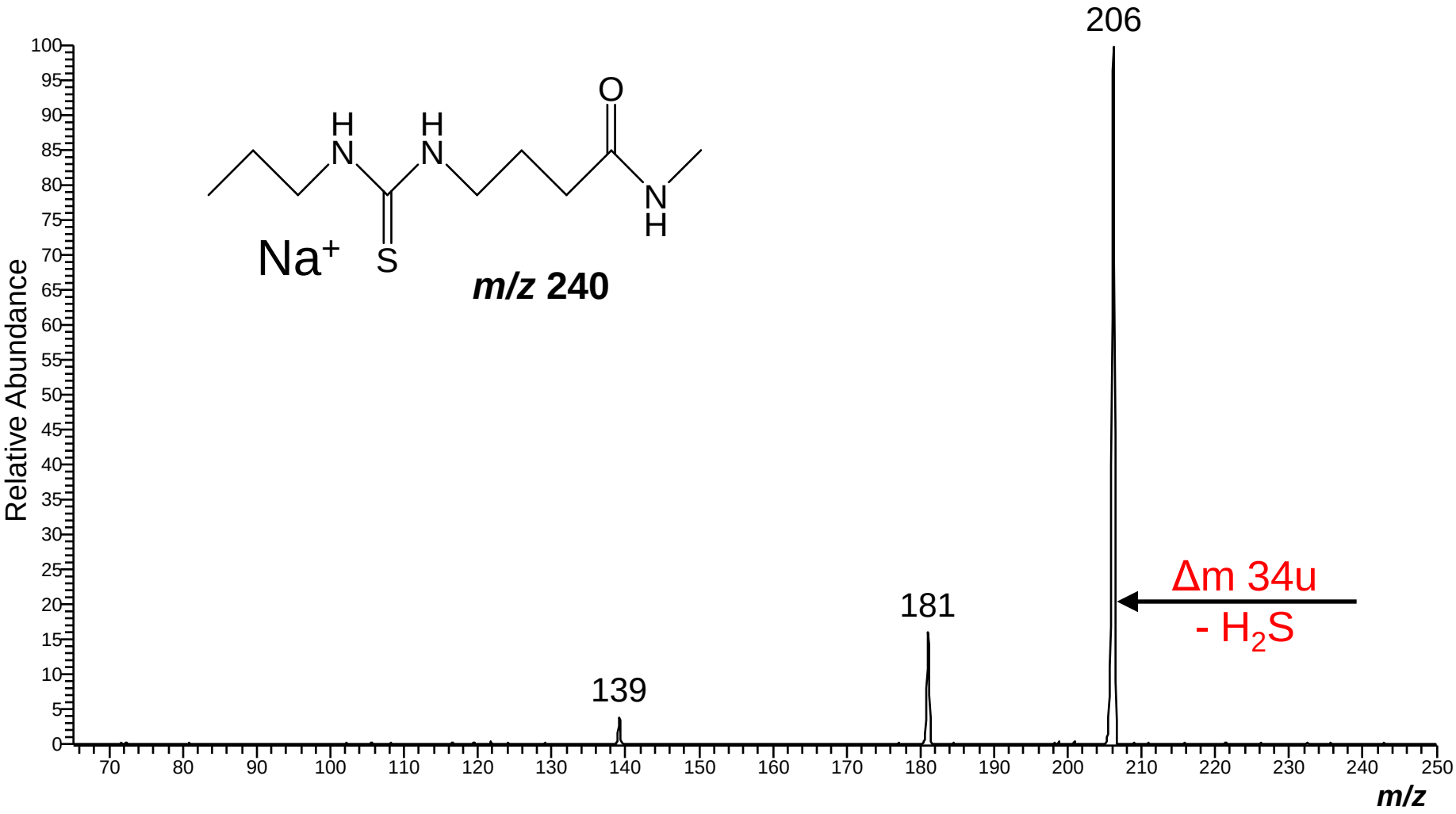


**Figure 2S:** (+)ESI-QIT-MS$^2$ product ion spectrum of the sodiated precursor ion [**3** + Na]$^+$ at *m/z* 240. The precursor ion is completely depleted by CID.

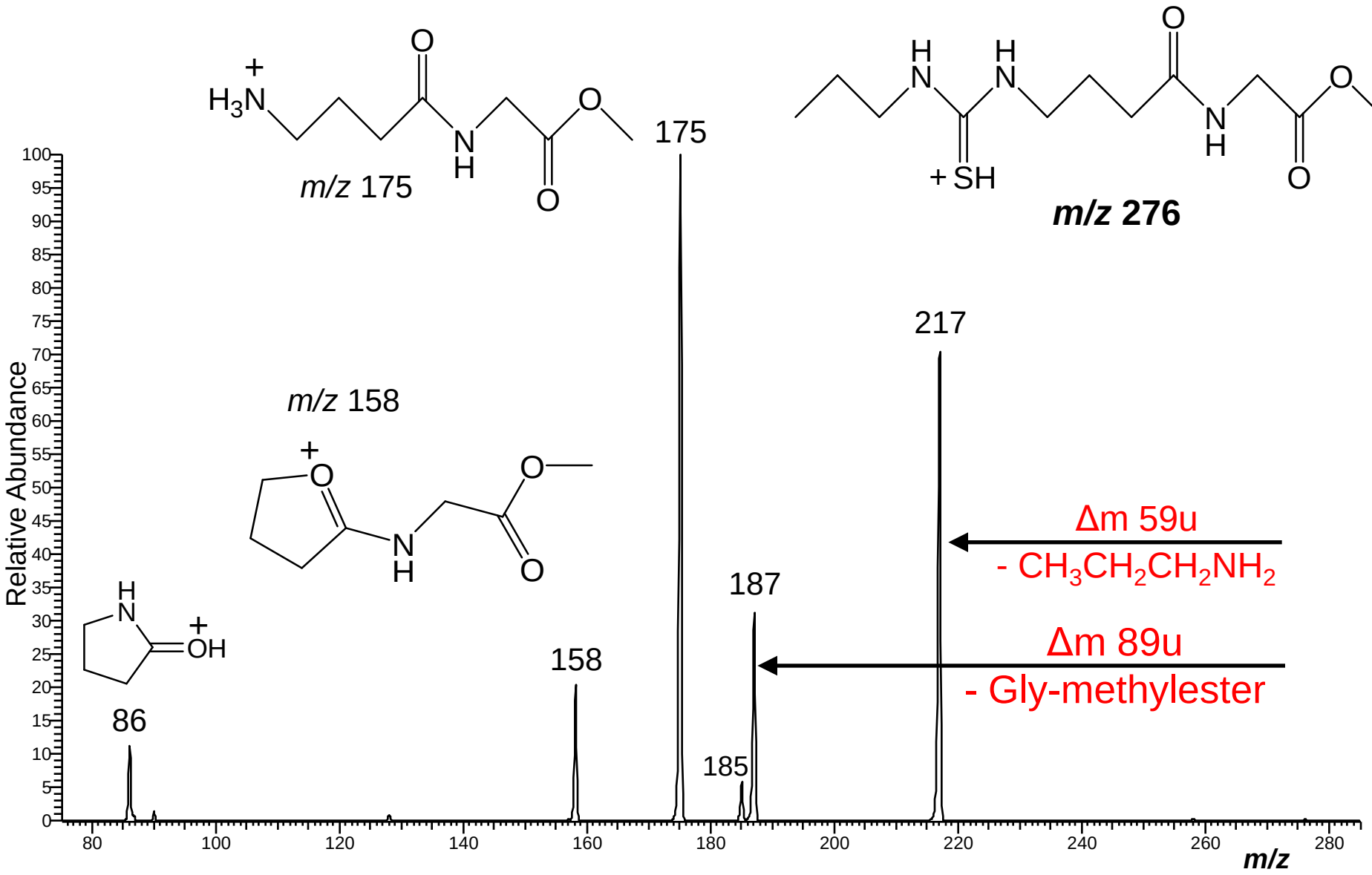


**Figure 3S:** (+)ESI-QIT-MS$^2$ product ion spectrum of the protonated precursor ion [**4** + H]$^+$ at *m/z* 276. The precursor ion is completely depleted by CID.

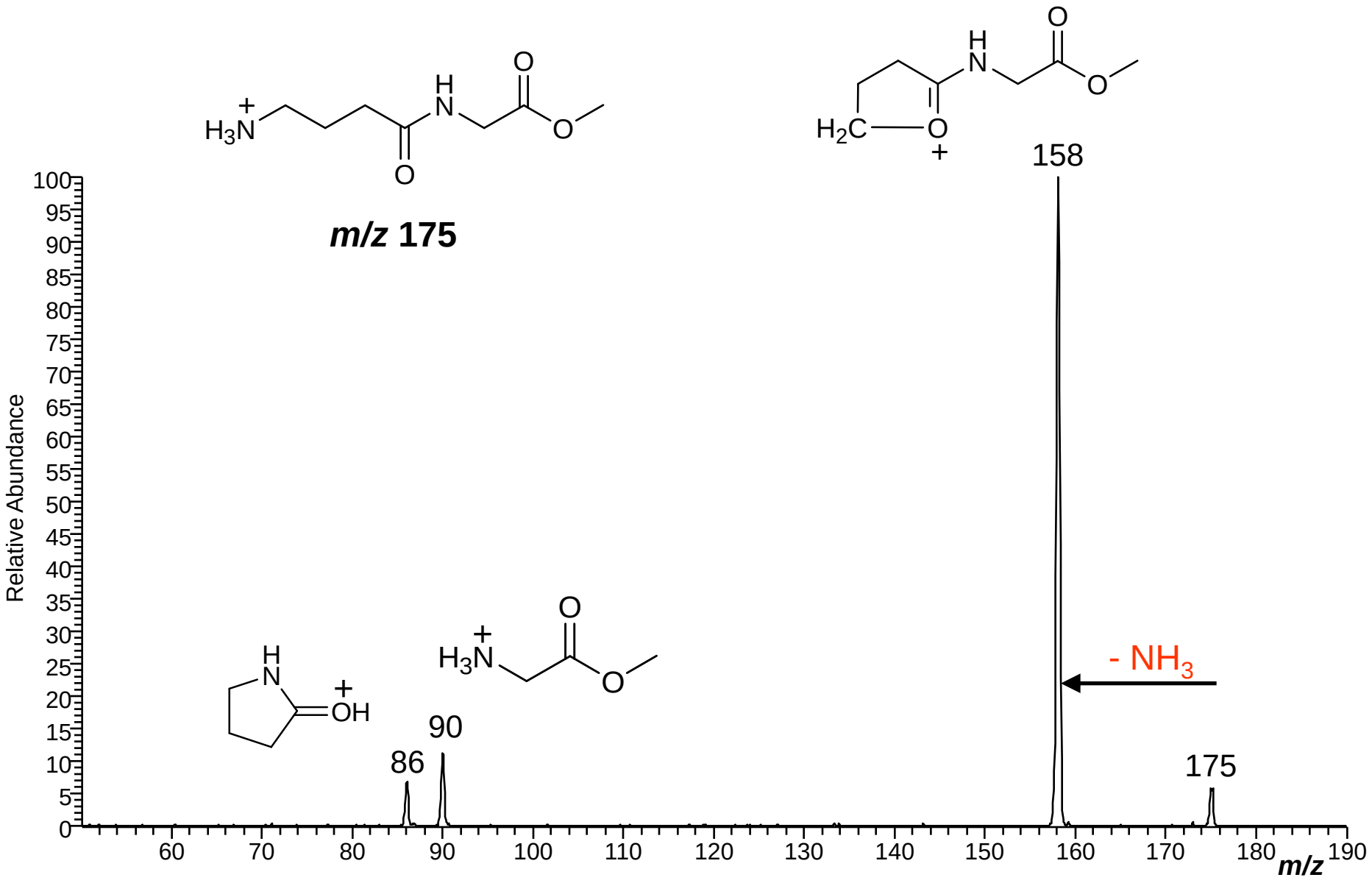


**Figure 4S:** (+)ESI-QIT-MS$^3$ product ion spectrum of *m/z* 175 generated by CID of the protonated molecular ion [**4** + H]$^+$ at *m/z* 276. MS$^3$: *m/z* 276 → *m/z* 175 →

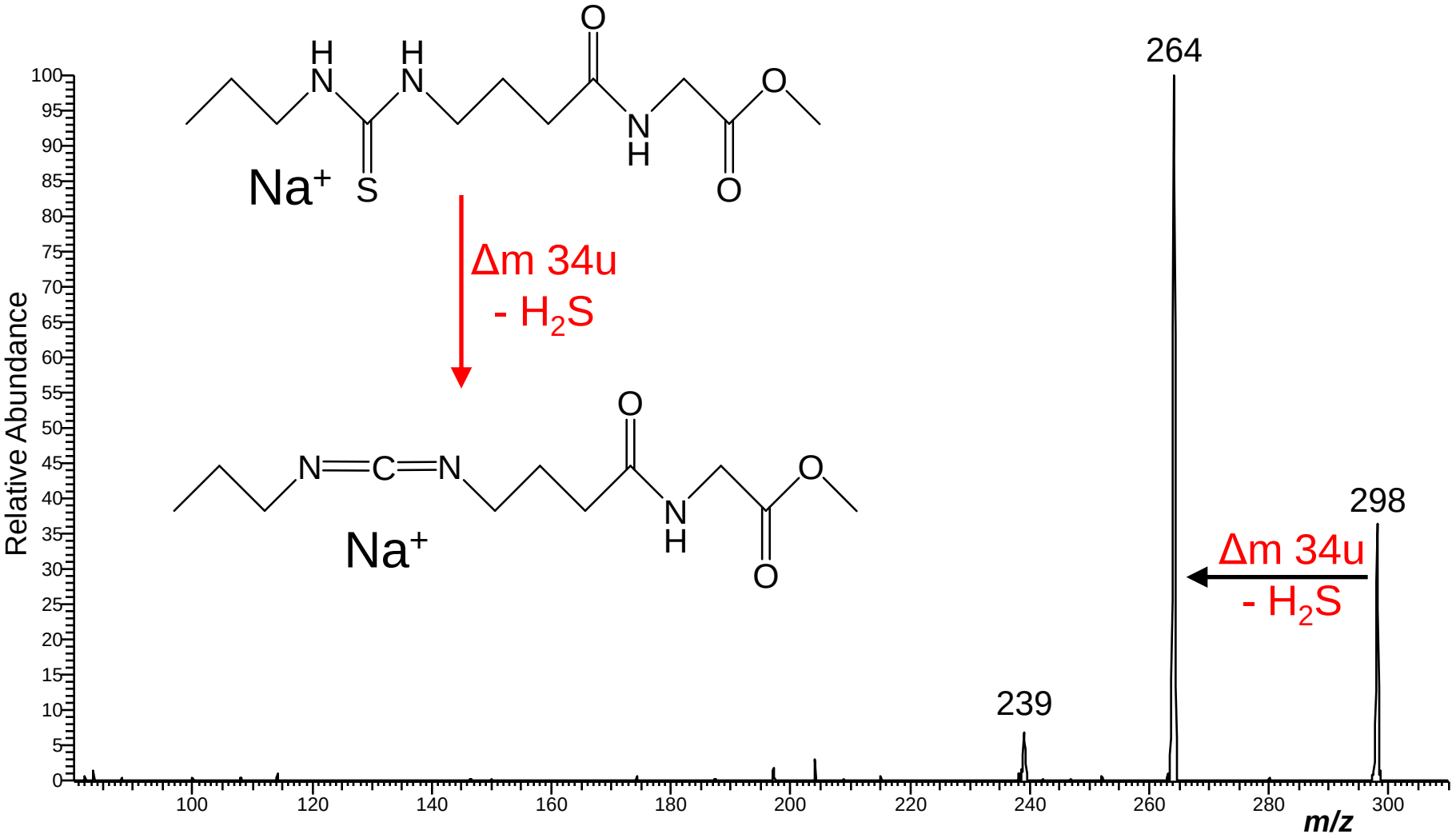


**Figure 5S:** (+)ESI-QIT-MS$^2$ product ion spectrum of the sodiated precursor ion [**4** + Na]$^+$ at *m/z* 298.

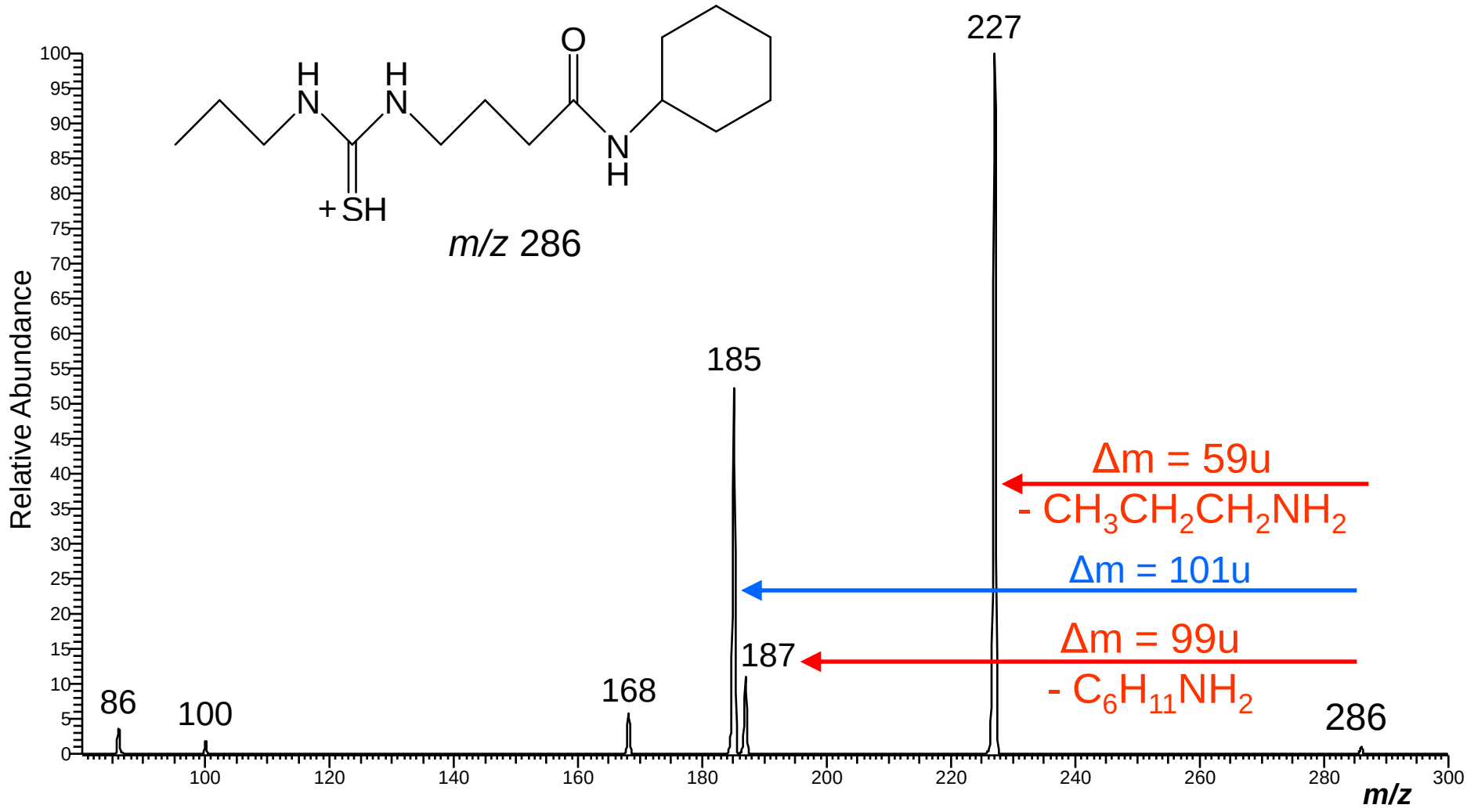


**Figure 6S:** (+)ESI-QIT-MS$^2$ product ion spectrum of the protonated precursor ion [**5** + H]$^+$ at *m/z* 286.

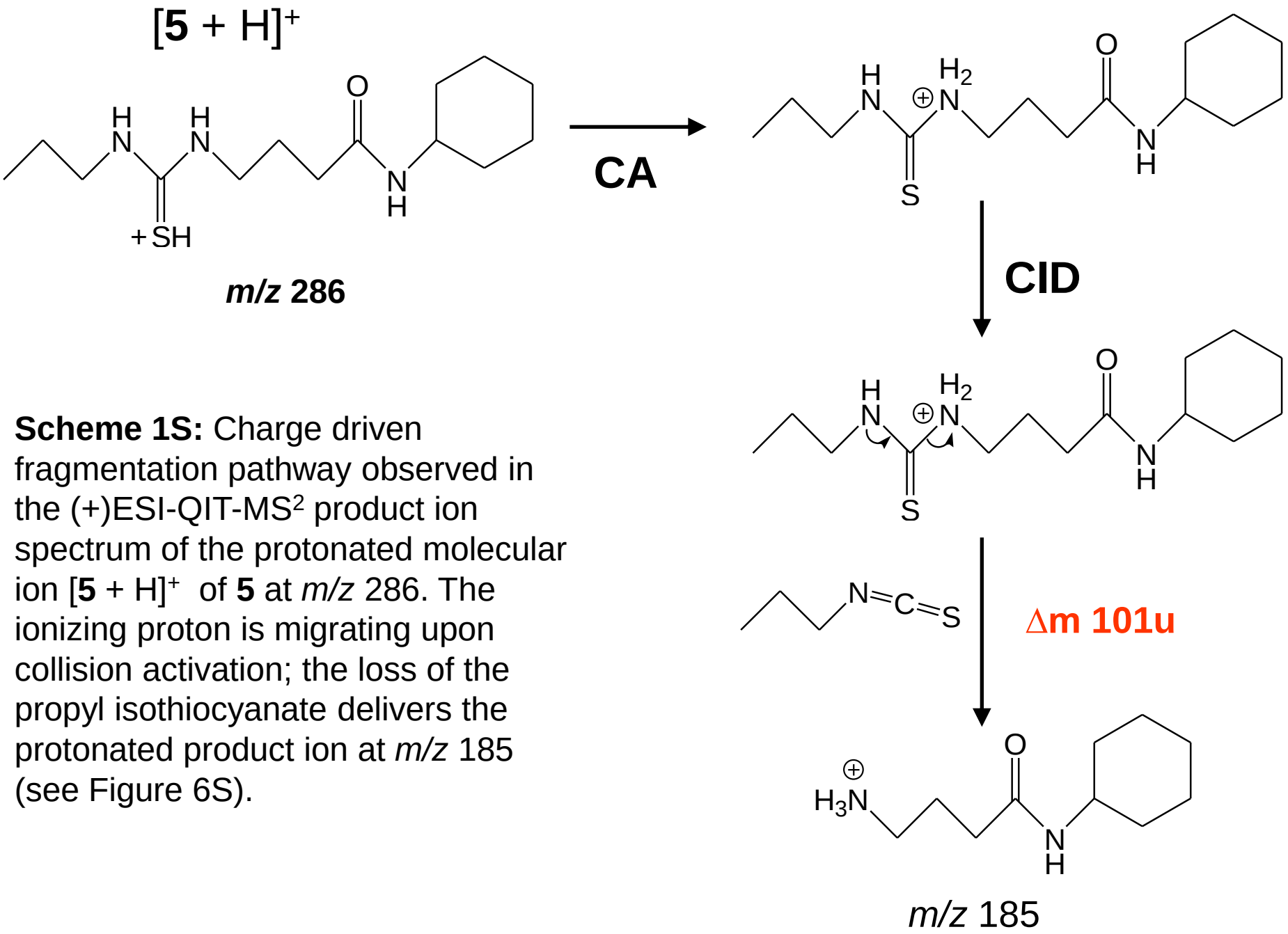


**Scheme 1S:** Charge driven fragmentation pathway observed in the (+)ESI-QIT-$MS^2$ product ion spectrum of the protonated molecular ion [**5** + H]$^+$ of **5** at *m/z* 286. The ionizing proton is migrating upon collision activation; the loss of the propyl isothiocyanate delivers the protonated product ion at *m/z* 185 (see Figure 6S).

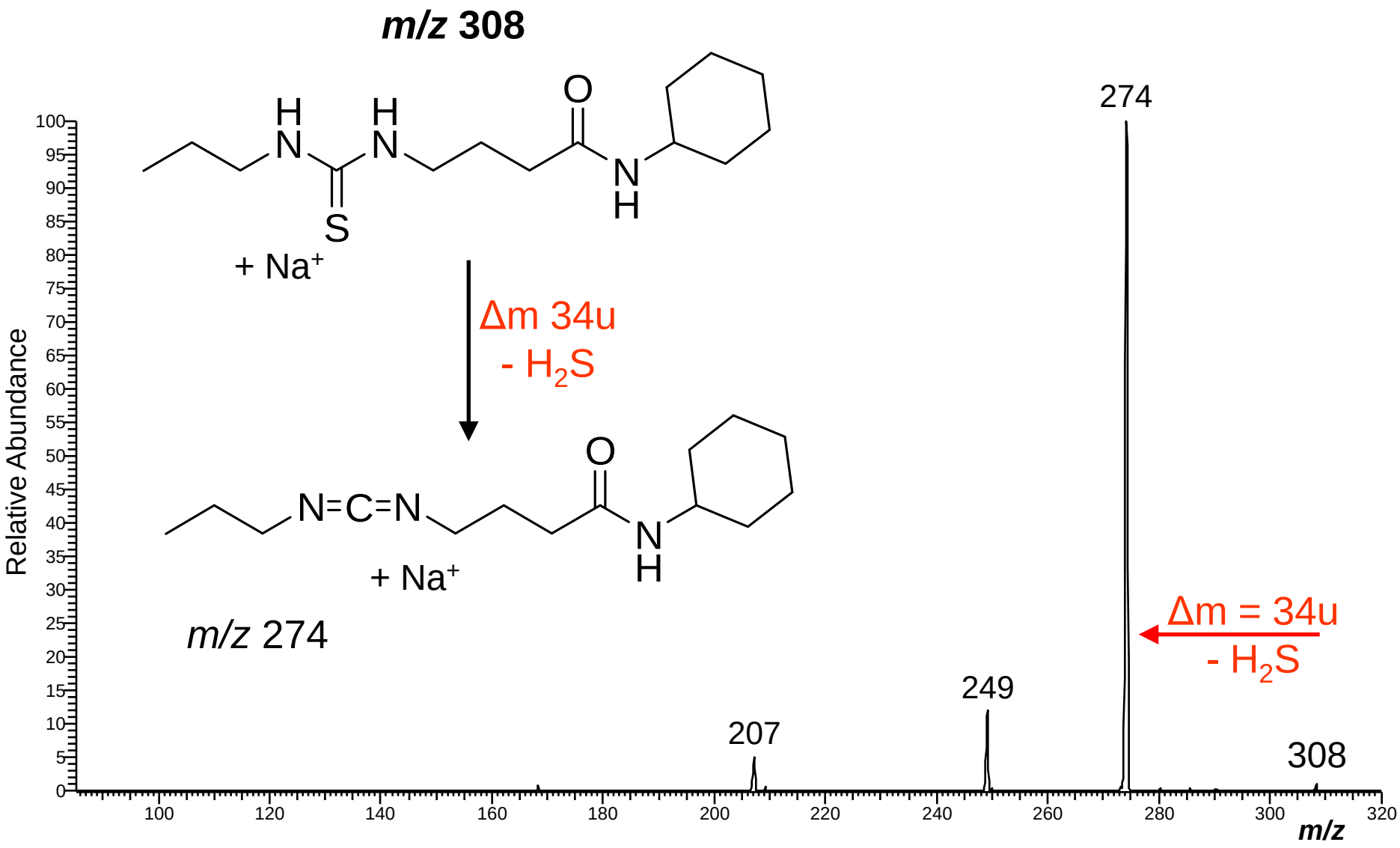


**Figure 7S:** (+)ESI-QIT-MS$^2$ product ion spectrum of the sodiated precursor ion [**5** + Na]$^+$ at *m/z* 308. The loss of 34 u correlates with the loss of hydrogen sulfide and the formation of the sodiated carbodiimide ion at *m/z* 274.

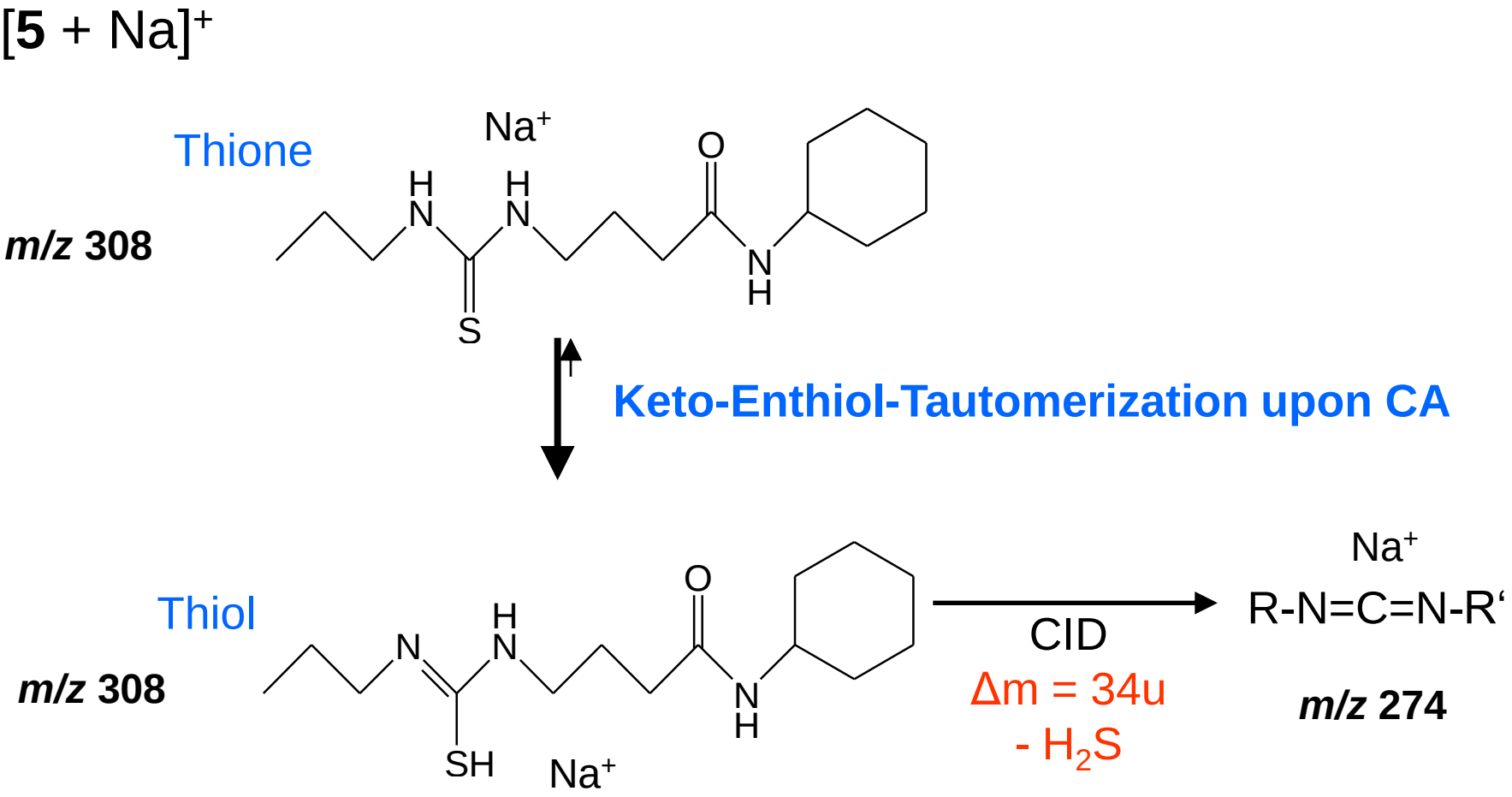


**Scheme 2S:** Thione-enthiol-tautomerization upon CA enables the loss of hydrogen sulfide and delivers the carbodiimide product ion at *m/z* 274 (see Figure 7S). The analogous reaction i.e. the loss of $D_2S$ (Δm = 36u) is observed with the triply labeled molecular ion [$D_3$**5** + Na]$^+$ at *m/z* 311 (see Figure 10S).

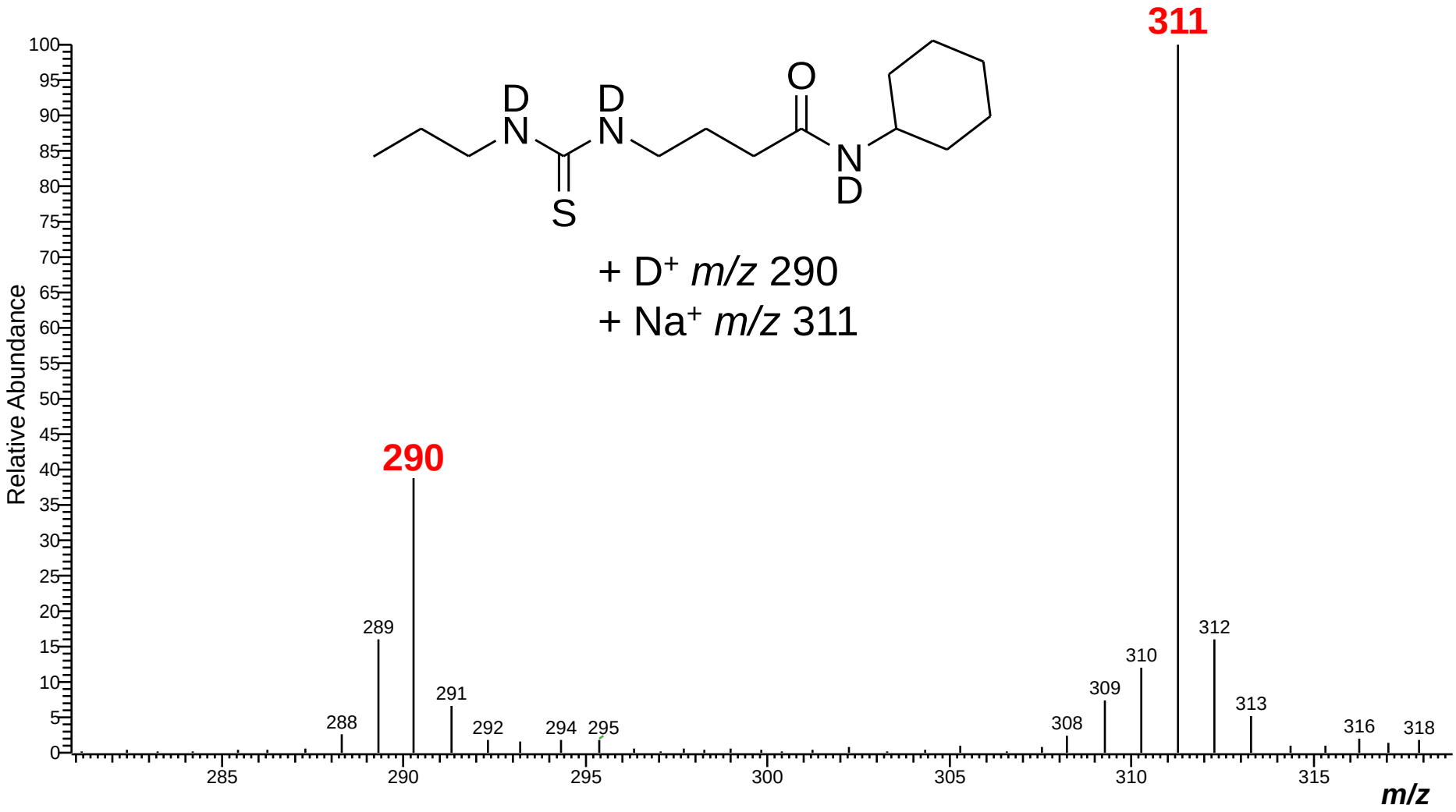


**Figure 8S:** Molecular ion region of the (+)ESI-Mass spectrum of compound **5** in deutero methanol/$D_2O$. The triply labeled molecular ions $[D_3\mathbf{5} + D]^+$ and $[D_3\mathbf{5} + Na]^+$ are found with prominent abundance at *m/z* 290 and *m/z* 311, respectively.

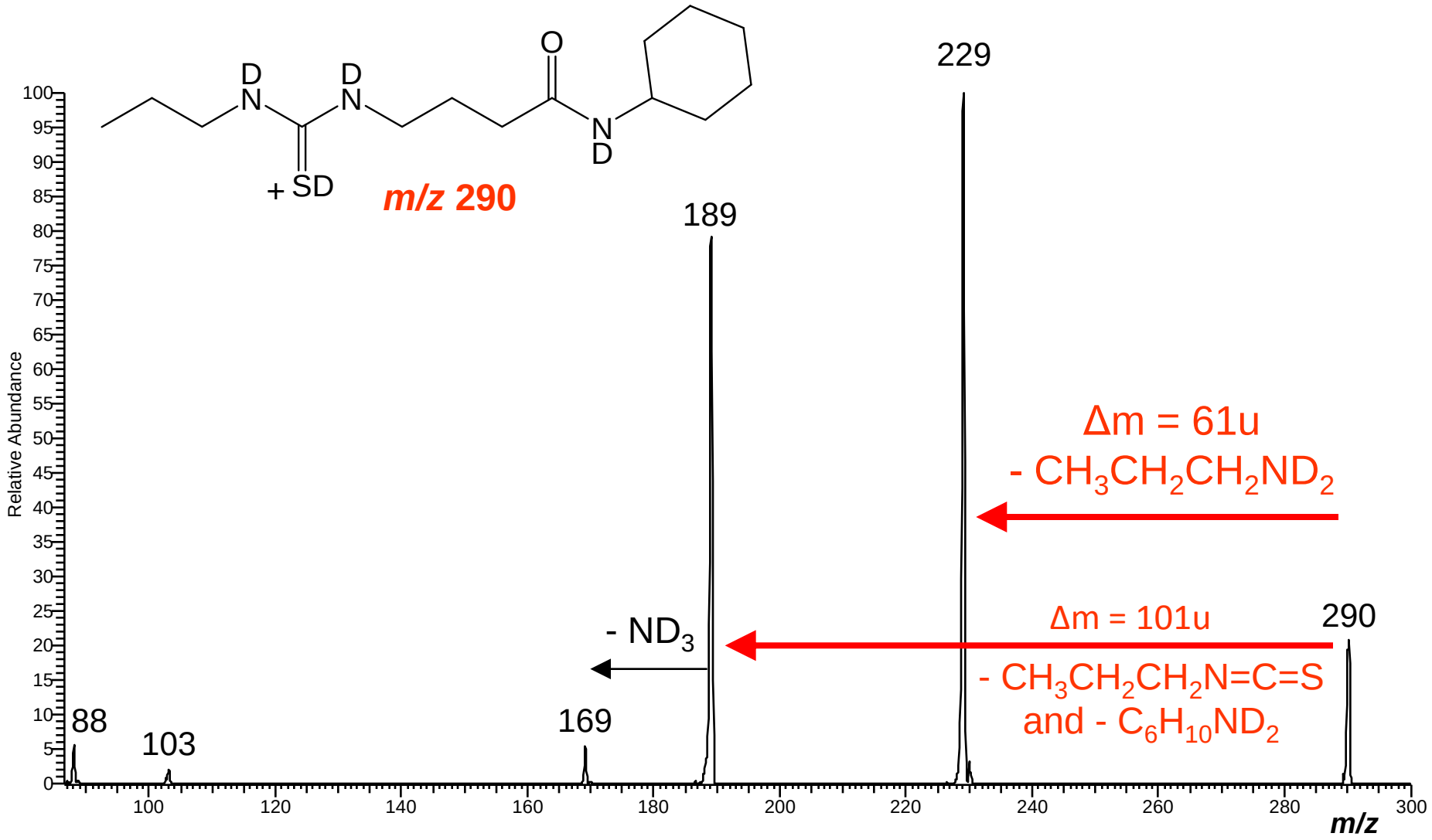


**Figure 9S:** (+)ESI-QIT-MS$^2$ product ion spectrum of the triply labeled $D_3$ precursor ion $[D_3\mathbf{5} + D]^+$ at *m/z* 290 generated by solving compound **5** in deutero methanol/$D_2O$. An analogous experiment with product ion analysis in the orbitrap confirms the composite character of product ion *m/z* 189

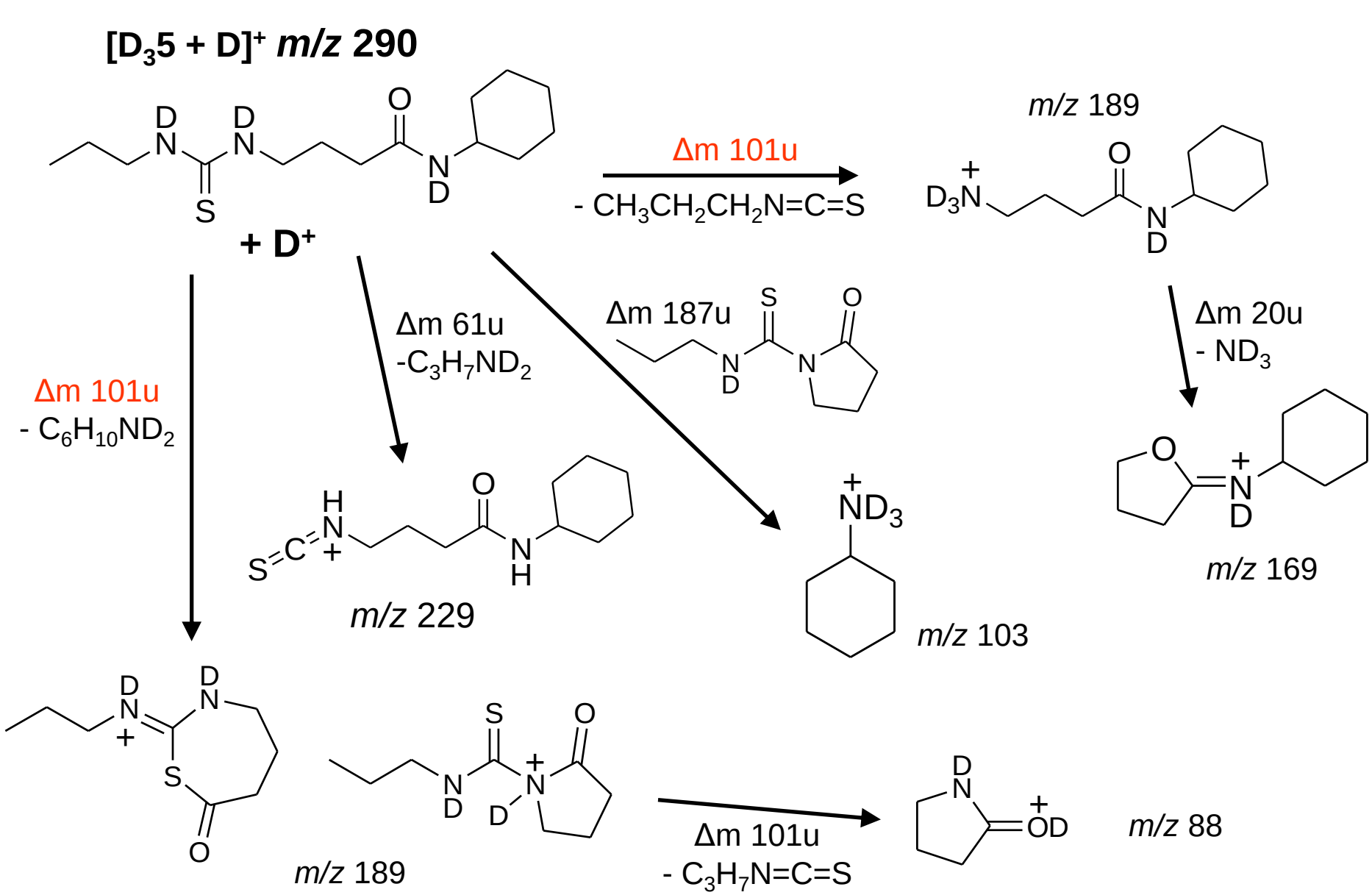


**Scheme 3S:** Charge driven fragmentation reactions observed in the QIT-MS$^2$ product ion spectrum of the labeled molecular ion $[D_3\mathbf{5} + D]^+$ at *m/z* 290 (see Figure 9S).

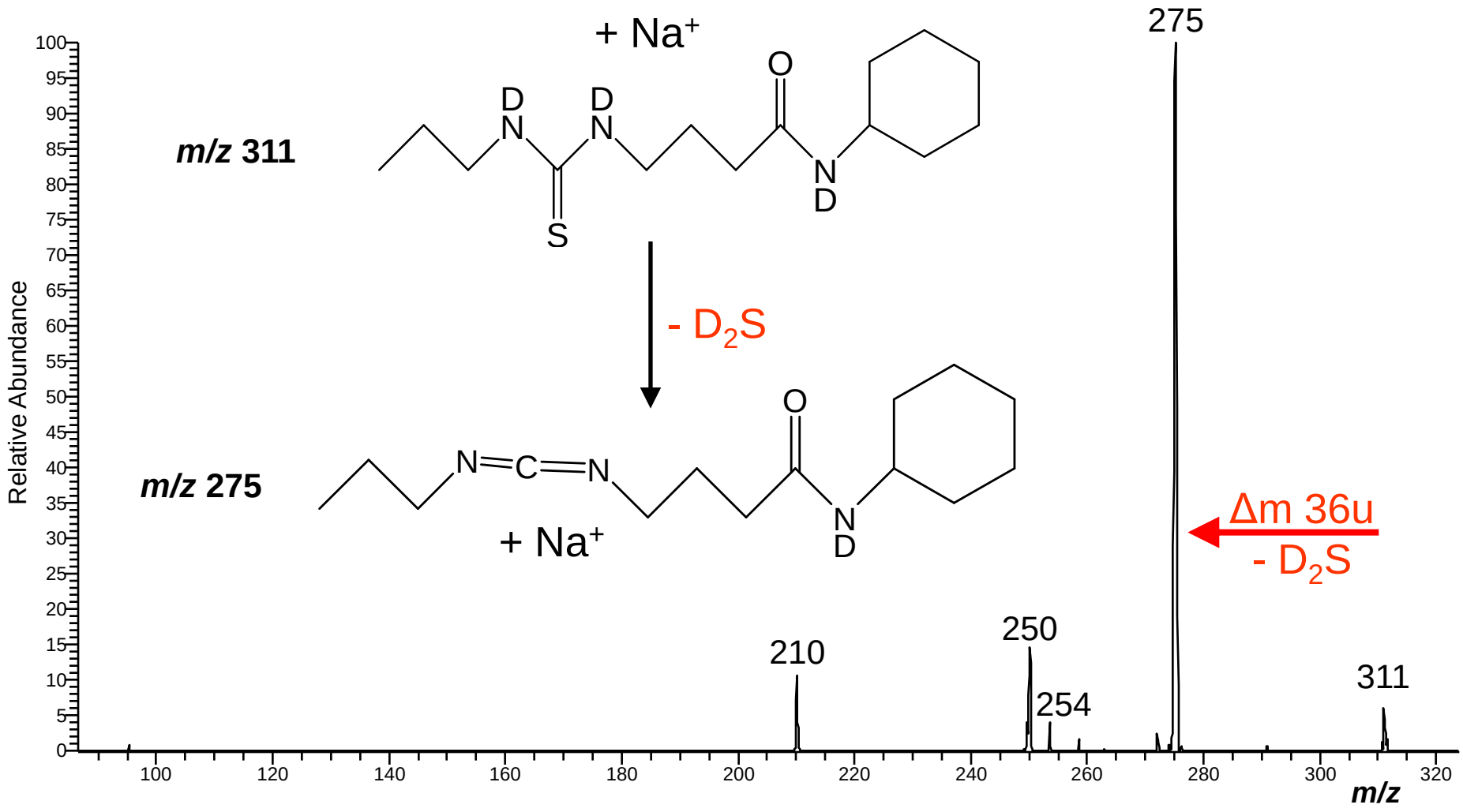


**Figure 10S:** (+)ESI-QIT-MS$^2$ product ion spectrum of the triply labeled $D_3$ precursor ion $[D_3\mathbf{5} + Na]^+$ at *m/z* 311 generated by dissolving compound **5** in deutero methanol/$D_2O$.

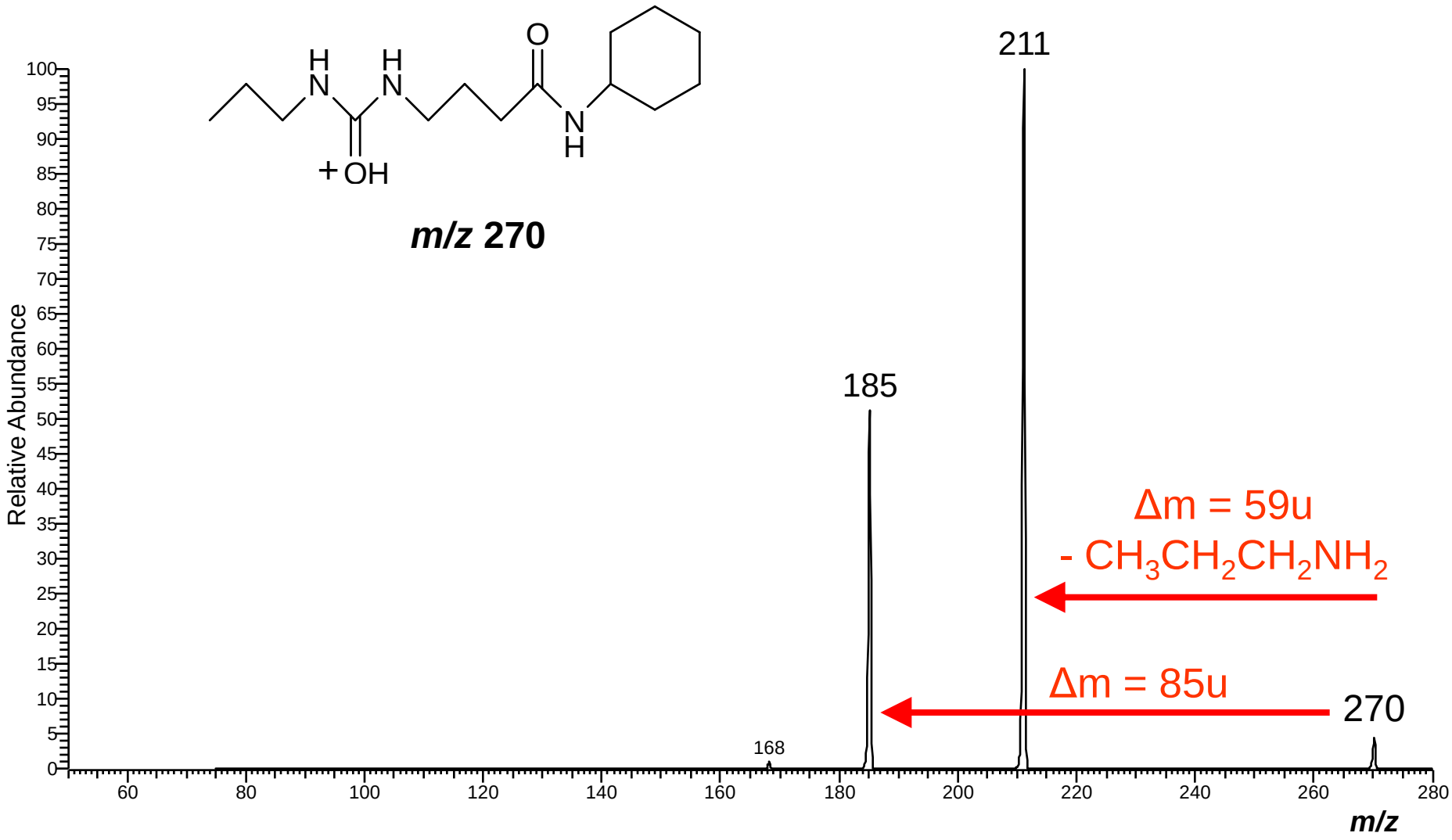


**Figure 11S:** (+)ESI-QIT-MS$^2$ product ion spectrum of the protonated precursor ion [**6** + H]$^+$ at *m/z* 270 ((+)ESI-MS: MeOH + 0.1%trifluoroacetic acid). The loss of 85 u is related to the loss of propylisocyanate (compare Scheme 1S).

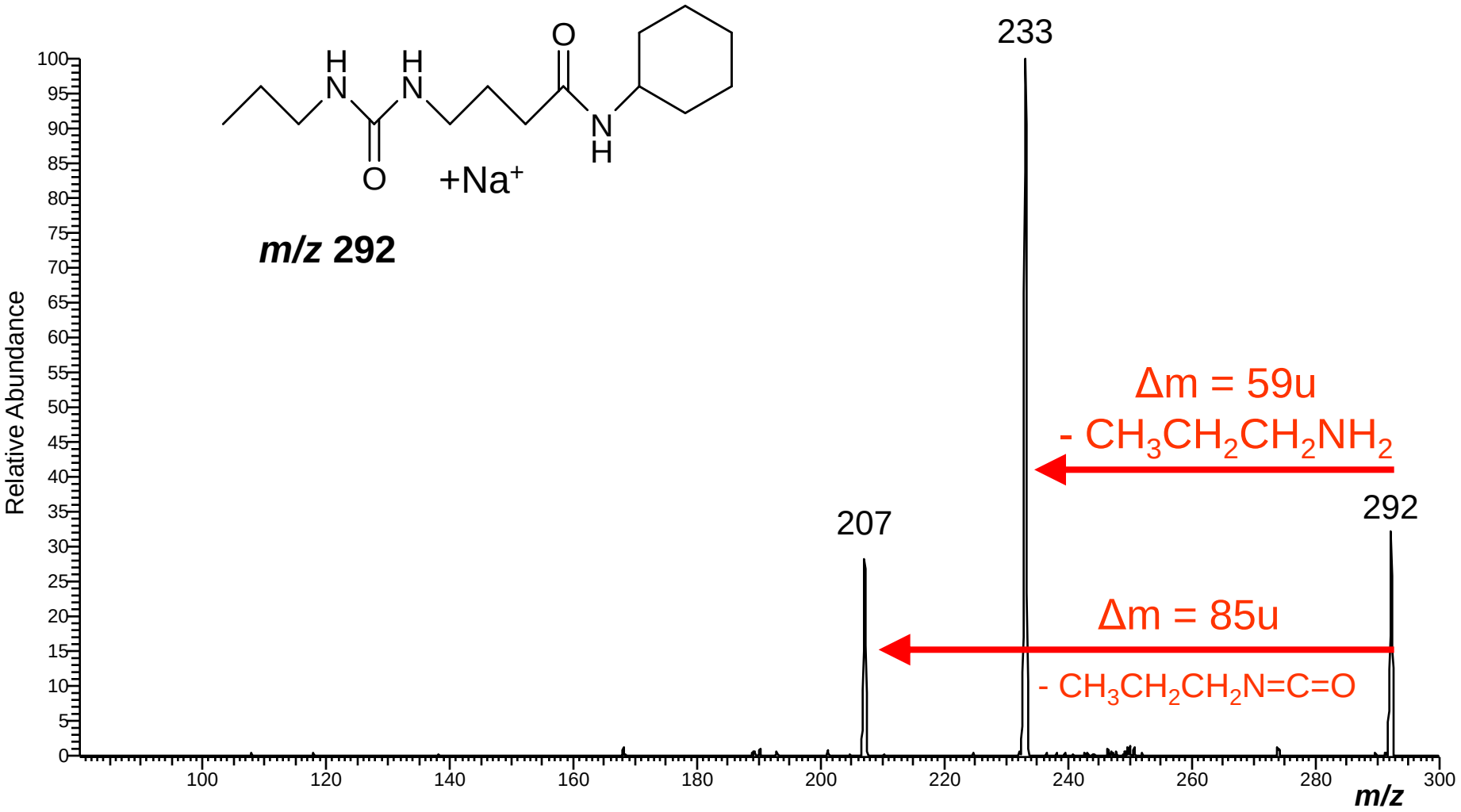


**Figure 12S:** (+)ESI-QIT-MS$^2$ product ion spectrum of the sodiated precursor ion [**6** + Na]$^+$ at *m/z* 292 from a methanol solution. The loss of 85 u is related to the loss of propylisocyanate (compare Scheme 1S).

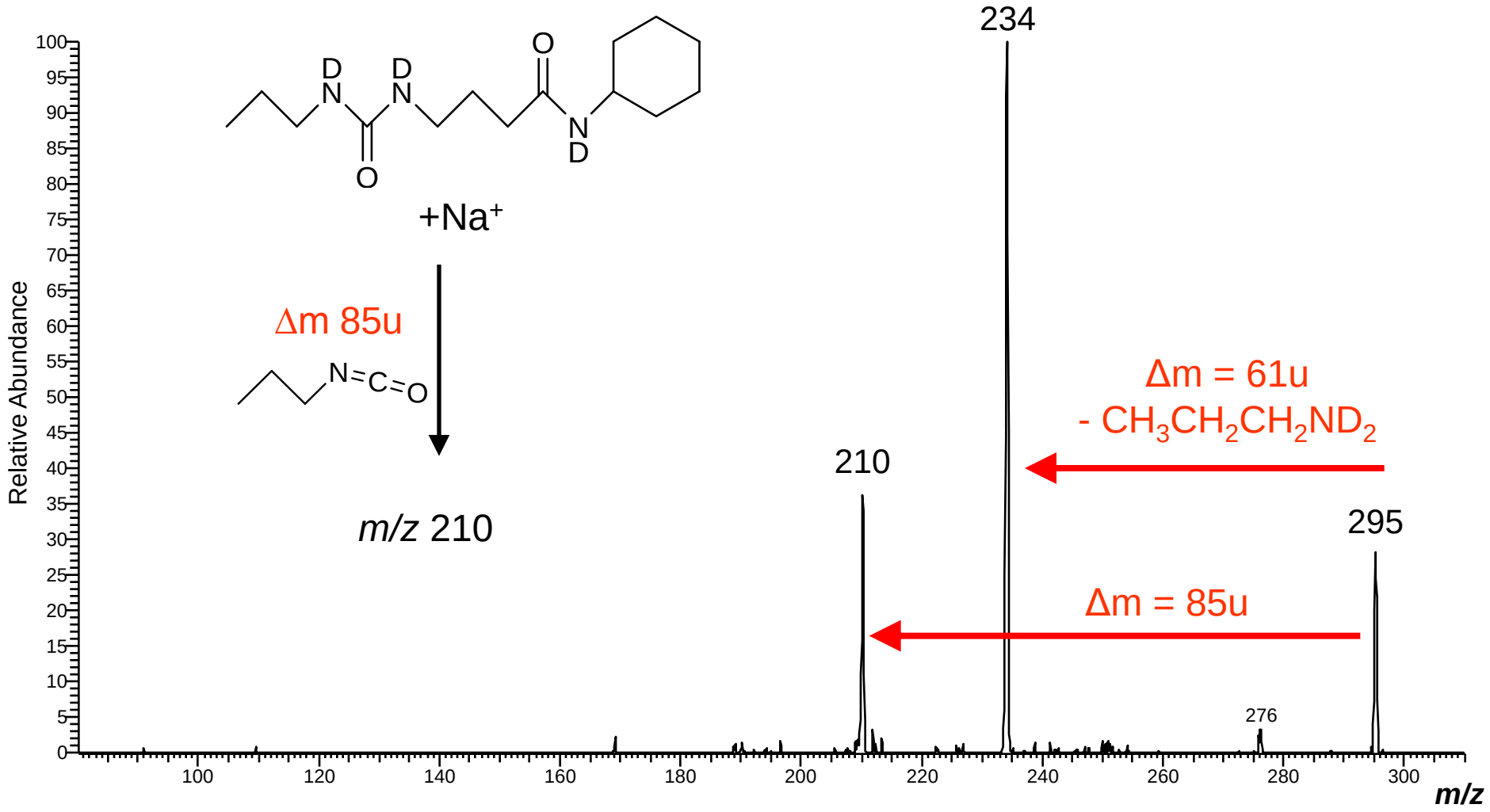


**Figure 13S:** (+)ESI-QIT-$MS^2$ product ion spectrum of the triply labeled precursor ion $[D_3\mathbf{6} + Na]^+$ at *m/z* 295, sprayed from a MeOD/$D_2O$ solution. The loss of 85 u is related to the loss of propylisocyanate. The absence of a mass shift (compare Figure 12S) evidences that no acidic proton is lost and hence, confirms the assignment.